UNIVERSITY OF THESSALY

SCHOOL OF ENGINEERING

DEPARTMENT OF CIVIL ENGINEERING

Master Thesis

INFLUENCE OF CONSTANT RESTORING FORCE ON THE DYNAMIC RESPONSE OF MULTI-STORY BUILDINGS

by

CHARALAMPOS ANDROULIDAKIS

A Thesis
Submitted in Partial Fulfillment of the Requirements for the
Degree of Master of Science in Civil Engineering
2011

ACKNOWLEDGMENTS

I would like to express my sincere gratitude to my advisor Associate Prof. Panagiotis Tsopelas for his support and guidance during my research experience, as well as to Prof. Eyripides Mystakides for the accommodation in the Construction Design and Analysis Lab.

One more personal note, I would like to thank my family for the mental support during all these years of study.

TABLE OF CONTENTS

SECTION	TITLE	PAGE

LIST OF FIGURES

LIST OF FIGURES (cont'd)

1.INTRODUCTION

The past 20 years a number of energy dissipation systems with constant restoring force, as the main component, have been proposed by engineers and researchers to minimize the structural damage in structural systems due to seismic motions. Constant restoring force can be achieved either through prestressing of structural elements (beams, columns, walls, and bridge piers) through tendons (Cheok and Stone, 1994; Mander and Cheng, 1997; Kwan and Billington, 2003; Kurama et al. 1999; Pampanin, 2005; Priestley and MacRae, 1996; Priestley and Tao, 1993; Mander, Contreras, and Garcia, 1998; Christopoulos et al. 2002; Christopoulos et al. 2008; Tremblay, et al 2008) or through pressurization of a fluid column in fluid based energy dissipation devices (Tsopelas and Constantinou 1994; Peckan et al. 1995; Pekcan, et al., 2000) Rocking based systems, which bridge piers and columns belong, have recently drawn considerable attention by researchers and engineers due to their potential for reduced fabrication and maintenance costs.

The effect of constant force as a restoring force mechanism in an energy dissipation system is investigated in this study. Multi story structural models are adopted in the study and are excited by two suites of seismic excitations, one representative of far-field and one representative of near-fault seismic motions. The main objective of the study is to investigate if the constant restoring force in energy dissipation systems is beneficial in reducing displacements of a structure (multi story frame) without resulting in increased story shear forces and floor accelerations, and how their performance compares to energy dissipation systems possessing displacement proportional restoring forces and damping mechanisms.

Section 2 presents in detail the characteristics of the two suites of the seismic motions considered in this study. Section 3 presents the considered energy dissipations systems and their corresponding devices. The fluid device with constant restoring force is presented analytically. For the other devices the main characteristics with their hysteresis loops are presented. At the end of this section the equivalent systems between them are constructed in order to have a clear view for the influence of the constant restoring force and the results can be comparable. In the next section the mathematical modeling for all the analysis that performed in this study is presented. At last are presented the results of the analyses in tables and comparing graphs.

A number of devices (Tsopelas and Constantinou 1994; Pekcan et al 1996) and systems (Christopoulos), have been proposed to reduce structural responses (displacements and/or forces) under dynamic excitations which have a strong "impact/high velocity" component. Such excitations are the near fault type of seismic motions as they have come into the earthquake and structural engineering research attention after the 1994 Northridge, 1995 Kobe, and 1999 Taiwan earthquakes.

In the present study the effect of constant restoring force of a seismic isolation system on the responses of a seismically isolated bridge model excited by near-fault motions is examined extensively. In order to evaluate that effect , the system responses (isolation system displacements, deck accelerations, pier accelerations, piers shear

1

forces) have to be compared to the responses of the isolated bridge when another seismic isolation system (e.g. viscoelastic in nature with linearly increasing restoring force) is utilized on the bridge.

Following this approach, one has to design/create a seismic isolation system which will provide similar isolation (stiffness or period) and energy dissipation (damping) properties to the isolation system with the constant restoring force. One has to recognize that designing such system might not be possible since an isolation system with constant restoring force has a highly non-linear behavior which can only be approximated (for a given level of displacement amplitude) by a system with effective properties, if the choice of a base system to compare against is a simple linear visco-elastic isolation system.

Two isolation systems consisting of two components are considered in the present study. The first component, which is common to both isolation systems, is the sliding bearings, which provide normal load carrying capacity as well as energy dissipation through friction. The second component, which is different for the two isolations systems and is presented for each one below, provides restoring force and viscous damping capacity.

- In the first isolation system Fluid Restoring Force and Damping Devices (FRFDD) providing constant restoring force and non-linear viscous damping capacity.

- In the second isolation system visco-elastic devices provide linear restoring force (linear spring) and linear viscous damping capacity.

1.1 Constant Restoring Force

The constant restoring force mechanism of a restoring force device or a damping device is depicted in Figure (1-1) as compared to the linear restoring force mechanism provided by a regular linear spring.

(a) Constant Restoring Force   (b) Linear Restoring Force
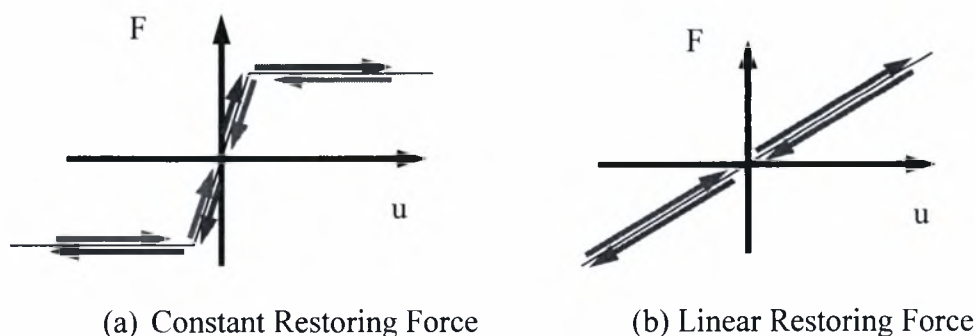
Figure (1-1) Force displacement relationships of a a) Constant Restoring Force Spring, and b) Linear Restoring Force Spring

The restoring force provided by a linear spring is proportional to displacements, implying that as the spring deformation increases/decrease the restoring force (the

2

spring imposes on the mass of a spring-mass dynamic system), increase/decresase. It is important to note that at the vicinity of the equilibrium position the restoring force for the linear spring takes very small values and the only force on the mass is the "inertial force" which can be seen as the velocity the mass is crossing (passing through) the equilibrium position.

When considering a Constant Restoring Force Spring (CRFS), the restoring force remains constant in amplitude throughout the motion/oscillation. This property has a significant effect in the behavior of a spring-mass system: at the vicinity of zero displacement the velocity which a mass crosses the neutral position is much larger than the velocity of a mass when the restoring force is provided by a linear spring. This can be easily seen considering the potential energy stored in the two springs at max deformation which in turn is transformed into kinetic energy at the equilibrium position.

The potential energy stored in a constant restoring force spring with force F_{max} and deformation u_o is : $E_{CRFS} \approx F_{max} u_o$ and the energy stored in a linear spring extended by the same deformation and reacting by the same force is : $E_{LS} = \frac{1}{2} F_{max} u_o$

From these energy expressions becomes clear that the potential energy to be transformed to kinetic energy, manifested by velocity, is almost twice for the constant restoring force spring. The velocity at the point of equilibrium in an oscillatory motion is very important since it is nothing more than the initial condition (initial velocity) for the motion of the mass when the displacement is zero (crosses zero). If that value is high then the maximum displacement which is going to be reached (in the following half cycle) in the oscillation in the direction of the velocity is going to be high also. To demonstrate this point, consider a SDOF system which undergoing free vibrations with initial conditions of velocity only. The system is going to deform more in the first cycle when the initial velocity is higher.

Exactly this point might be the one where an engineer has to be cautious when systems with constant restoring forces are used.

3

2.INPUT SEISMIC EXCITATIONS

The models used in this study were analyzed for two types of seismic motions. Firstly the analysis performed for far filed motions and secondly for near filed motions. In the next topics the characteristics of these excitations are presented in detail.

2.1 Far field seismic excitations

In the analysis were used 20 scaled far field seismic excitations, provided from the study of Tsopelas et al. (1997). The scaling process was presented in the study mentioned. These motions are the horizontal components of ten earthquakes. Table 2-1 presents these motions and their scale factors.

Table 2-1 Motions used in Analysis and Scale Factors

Year	Earthquake	Station	Components	Scale Factor
1949	Washington	325 (USGS)	N04W, N86E	2.74
1954	Eureka	022 (USGS)	N11W, N79E	1.74
1971	San Fernando	241 (USGS)	N00W, S90W	1.96
1971	San Fernando	458 (USGS)	S00W, S90W	2.22
1989	Loma Prieta	Gilroy 2 (CDMG)	90, 0	1.46
1989	Loma Prieta	Hollister (CDMG)	90, 0	1.07
1992	Landers	Yermo (CDMG)	360, 270	1.28
1992	Landers	Joshua (CDMG)	90, 0	1.48
1994	Northdridge	Moorpark (CDMG)	180, 90	2.61
1994	Northdridge	Century (CDMG)	90, 360	2.27

The earthquakes were selected to have magnitude larger than 6.5,epicentral distance between 10 and 20 km and site conditions of soft rock to stiff soil. The scaling performed in order to provide a balance contribution to the average response spectrum and preserves the frequency content. Figure 2-1 presents the average, maximum and minimum response spectrums of the 20 scaled motions comparing to the target NEHRP design response spectrum. Figure 2-1 demonstrates the variability in the characteristics of the scaled motions, which is implicit in the definition of the seismic hazard.

4
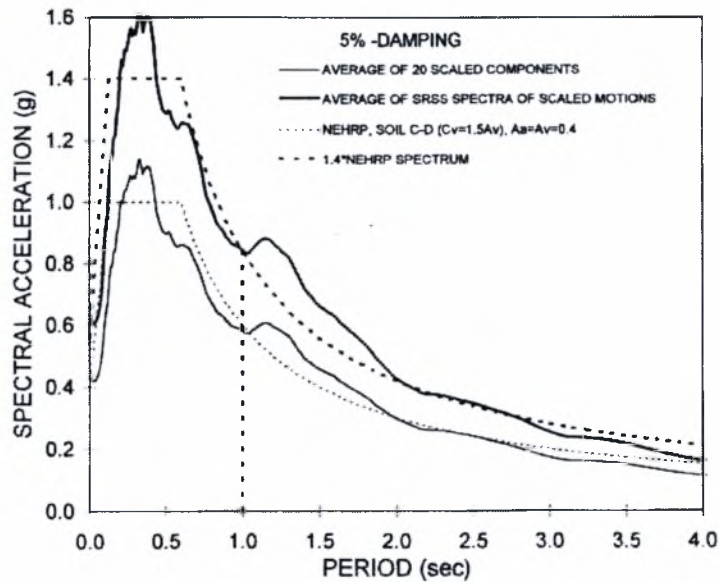
Figure 2-1 Maximum, average and minimum spectral acceleration values of scaled motions (from Tsopelas et al. 1997)

2.2　Near field seismic excitations

Near- field ground motions

Earthquake ground motions could be classified as near-field (fault) and far-field and their destructive potential in a certain location, depends on event's magnitude, source characteristics, distance and direction from the rupture location and local soil conditions. Far-field motions are characterized from high frequency signal and sharp acceleration records while near-fault motions result to large ground displacements, from 0,5 m to more than 1 m, with distinct pulses in their velocity and displacement records. Near-fault motions and their effect on seismically-isolated structures, long-span bridges and flexible buildings have gained considerable attention from earthquake engineering researchers.

First Housner and Trifunac (1967) identified, from the 1966 Parkfield, California earthquake, the coherent long period pulses in velocity and displacement time histories, dissociating this record from a typical far-field signal. Then such the existence of these pulses are verified from a representative data set of recorded ground motions worldwide, Bertero et al. (1978) observed the severe implications on flexible structures, when after the 1994 Northridge California earthquake this scientific area was accepted from the majority of engineers.

Near-fault motions are the result of stress waves moving in the same direction as the fault ruptures, thereby being crowded together to produce a long-duration pulse

5

(Nikos Makris). Although the large collected records from stations located near the causative fault, these intense pulses are not distinguished in the majority of the records. Effects as directivity and fling are often responsible for the pulse generation furthermore the relative position of the station that recorded the motion with respect to the direction of propagation of the rupture front on the fault plain is employed with the pulse existence (George P. Mavroeidis and Apostolos S. Papageorgiou)[MSOffice1]

2.2.1 Directivity effect

Directivity effect is related to the direction of the rupture front and it is distinguished as forward and backward directivity. Forward directivity observed when the site is away from the epicenter (it can be near the fault) and the rapture front propagates toward the site, where the station is located. Backward directivity occurs when the site is near the epicenter and the rapture propagates away from it. The velocity pulse is characterized by a positive and negative swing (reversing pulse), caused by the constructive interference of SH waves, generated from the parts of the rapture, which are being activated in an earthquake. The finite time that the rapture occurs is responsible for this effect. Another feature of directivity effect is the under-predicted incoming pulse from the attenuation-relation models when the rupture propagates toward to the site, while for the reverse case more conservative pulse would be predicted. In addition with the far-field records, where the strong horizontal component seems to be random, in directivity effect the strong components is constantly appeared in the strike-normal direction, for strike-slip and also for dip-slip faults. It is expected, from definition that the coherent pulse perpendicular to the strike to be larger.

2.2.2 Fling Effect

Fling is related to the permanent tectonic deformation at a site, which is located near the fault with distance mindless from the epicenter. In ground-displacement record, a permanent offset of the ground is identified as fling effect. The velocity time history plot is characterized by a one-sided velocity pulse, which in the strike-slip faults, is associated with the fault-parallel component. Fling for the strike-slip and dip-slip faults, is associated with the fault-parallel and fault-normal component, respectively.

6

3.DAMPING DEVICES

When structures are subjected to dynamic loadings, such as seismic motions, a large amount of energy is coming into the structure. This energy if there is no other mechanism to absorb it in the structure could be potentially absorbed by structural members through inelastic behavior and damage. The last two decades engineers have been developing devices and systems which improve the dynamic response of the structures and make them able to survive from destructive earthquakes by absorbing the seismic energy entering the structures. These devices could be friction dampers, solid visco-elastic dampers, steel yielding dampers, linear or nonlinear fluid viscous dampers and others.

The force deformation characteristics of any damping device has a form of hysteresis/loop, with the enclosed area in a cycle of motion representing the energy dissipated by the damping mechanism or mechanisms of the device.

This section is presenting in detail the fluid restoring force/ damping device considered in this study as well as the main characteristics of other energy dissipation systems which are also examined in this study. Finally, the method for developing equivalent damping systems to the one with the constant restoring force mechanism is presented.

3.1 Fluid Restoring Force/Damping Device

These devices are placed between two successive floors of a building structure. The fluid restoring force/damping device (FRFDD) and its construction is shown in Figure 3-1. Typical force-displacement loops of one device under static and dynamic loading conditions are presented in Figure 3-2.

Each device features a preload F_o, stiffness K_o (slope for forces exceeding the preload) and a viscous force component. Furthermore, the device is double-acting with the identical properties in tension and compression.
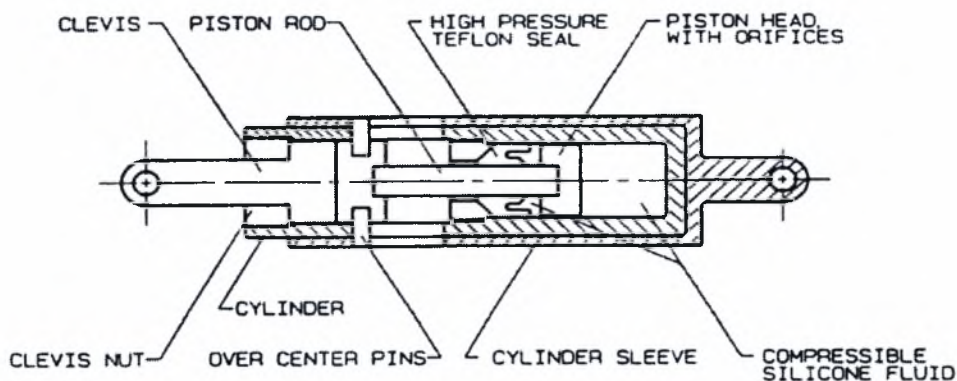
Figure 3-1 Construction of Fluid Restoring Force/ Damping Device

7
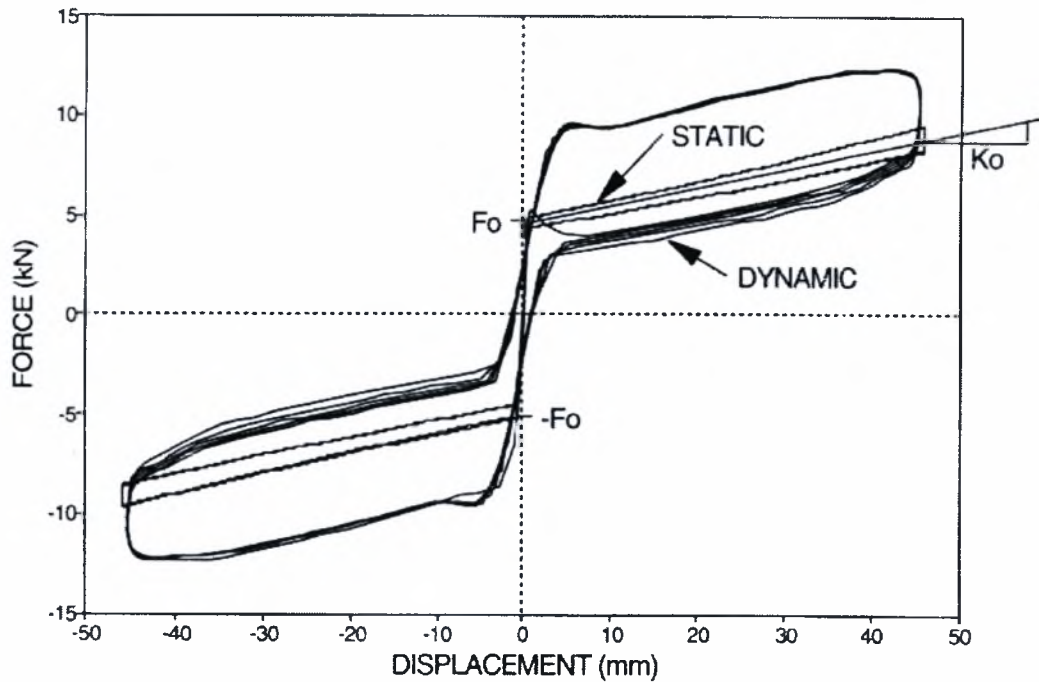
Figure 3-2 Force- Displacement Relationship of FRFDD

The devices are compressible fluid springs which are pressurized in order to develop the preload. Furthermore, fluid orificing is utilized to produce viscous damping force. The principles of operation of the devices are illustrated in Figure 3-3. A hydraulic cylinder is completely filled with silicon oil. A rod of area A_r is forced into the cylinder. Thus, the volume of the fluid is reduced by $A_r u$, u being the imposed rod motion. The overpressured p in the cylinder is

$$p = \frac{F}{A_r}$$

(3-1)

and is related to the volume change $\Delta V = A_r u$

$$p = K \frac{\Delta V}{V}$$

(3-2)

where, K is the fluid bulk modulus and V is the fluid volume.
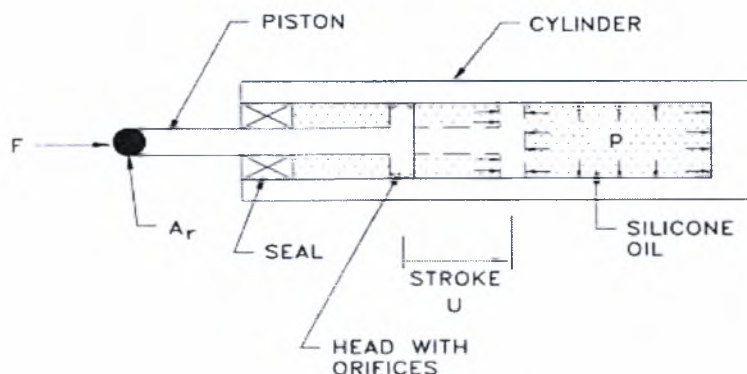
Figure 3-3 Principles of operation of FRFDD

8

Therefore,

$$F = \frac{KA_r^2}{V}u \tag{3-3}$$

This relation is depicted in Figure 3-4(a). In general, this relation is nonlinear due to the dependency of the bulk modulus to the total pressure p_T and the fact that volume V is not constant but rather equal to $V_0 - A_r u$, where V_0 is the fluid volume at zero displacement. More accurately, Equation (3-3) should be written as

$$F = \int \frac{K(p_T)A_r}{V_0 - A_r u}du \tag{3-4}$$

where $K(p_T)$ is the pressure dependent in bulk modulus.

Friction in the seal of the devices alters the force-displacement relation to the form depicted in Figure 3-4(b). By pressurizing the device to an initial pressure of p_0, a preload F_0 develops

$$F_0 = A_r p_0 \tag{3-5}$$

This preload must be exceeded for the rod to move. The resulting force-displacement relation is shown on Figure 3-4(c).

9
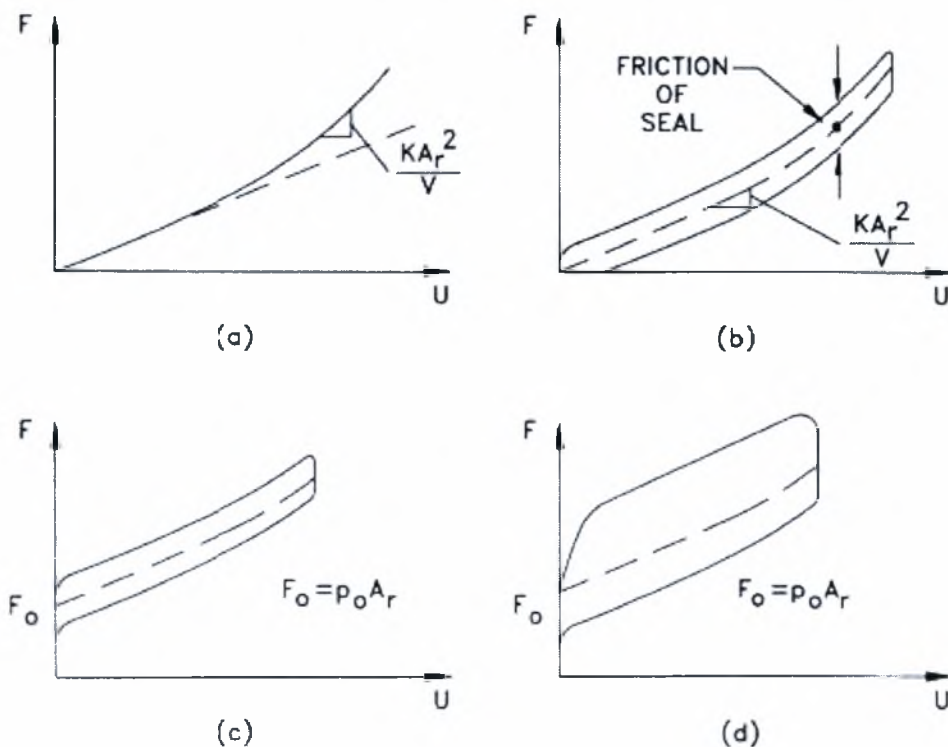
Figure 3-4 Components of FRFDD

This piston head supports the rod and provides resistance to fluid transfer across the head during stroke. The area and shape of the orifices on the piston head determine the level and nature of the developed viscous forces. This viscous forces are, of course, related to the velocity of the piston rod. A complete force-displacement loop is depicted in Figure 3-4(d). It may be noted that the loop in this figure is shown with the viscous force being more in one direction than the opposite direction. This behavior is produced by utilizing additional orifice area in only one direction. The behavior is desirable because it provides high damping force when the stroke increases, that is when needed, while it provides low damping force on return. This behavior however, might lead to unwanted large velocities as the device is returning towards and passing through its equilibrium position, since it might not be slowed down enough as discussed previously.

This type of compressible fluid restoring force/damping device has been used by U.S.Military since the 1970's. The device that was used in these tests is virtually the same as that used as the arresting hook centering spring-damper on the carrier based Lockheed S-3 Viking aircraft. Other applications include those of weapons grade shock isolation systems for the NATO MK49 ring laser gyro navigator, the shipboard version of the sparrow missible, the MX missible and the Seawolf submarine. Output force ranges for these applications are between 1 and 1500 KN.

Furthermore, compression-only versions of these devices with designs dating prior to 1970 are still used as shock absorbers in industrial applications. Moreover, such compression-only shock absorbers have been used in a number of bridge applications in Italy (Greiner 1991). The devices were used as shock absorbers for preventing impact of the deck on the abutments. One application described by Greiner, 1991 is on a 25000 ton bridge which utilized four compression only shock absorbers, each with 500 ton peak output force at displacement of 500 mm.

3.1.1 Analytical Model for Fluid Restoring Force/Damping Devices

The force in a restoring force/damping device consists of a preload (the constant restoring force), a mild restoring force proportional to the displacements, the friction force at the seal and the fluid damping force. Section 3.3 presents a discussion on the origin of the components and Figure 3-7 illustrates these components. The four components may be mathematically expressed as follows:

$$F_t = F_0 \left[1 - \exp\left(-\delta|u|\right)\right] \text{sgn}(u) + K_0 u + \left[F_{\min} + \zeta K_0 |u|\right] Z_t + F_d \text{sgn}(\dot{u}) \tag{3-6}$$

$$F_d = F_1 \left(\dot{u}\right) \quad \text{when } u\dot{u} > 0 \tag{3-7a}$$

$$F_d = F_2 \left(\dot{u}\right) \quad \text{when } u\dot{u} < 0 \tag{3-7b}$$

in which F_0 is the preload, K_0 is the stiffness, $F_{\min}$ is the seal friction at zero displacement and F_d is the fluid damping force, which depends on velocity and

10

direction of motion. Furthermore, Z_t, is a hysteretic variable governed by the following equation:

$$Y_t \dot{Z}_t + \gamma |\dot{U}_t| Z_t |Z_t| + \beta \dot{U}_t Z_t^2 - U_t = 0 \tag{3-8}$$

u is the device displacement and u' is the device velocity (actually displacement and velocity of one end of the device with respect to the other end).

The term $\zeta\, K_0\, |u|$ accounts for increased friction in the seal as a result of increased internal pressure during stroking. The seal typically consists of very soft material that cold flows under the internal pressure to seal microscopic surface finish patterns. Thus as pressure increases during stroking, so does friction. Herein we use a linearly increasing friction force based on the experimental results. Furthermore, we selected a linear restoring force $(K_0 u)$ as an acceptable approximation to the actual condition, which has a mild nonlinear behavior. The physical origin of this nonlinearity has been explained previously.

The preload term should, for ideal conditions, be presented by a term $F_0 \operatorname{sgn}(u)$. In reality, the stiffness of the device is not infinitely large at zero displacement. Rather, it is dependent on the velocity of motion of the piston rod. This behavior is accounted for in the model by the exponential term for the preload $F_p = F_0 \left[1 - \exp(-\delta |u|) \right] \operatorname{sgn}(u)$, in which δ is a function of velocity. The experimental results suggest an exponential form for variable δ:

$$\delta = \delta_0 \cdot \exp\left(-\delta_1 |\dot{u}|\right) \tag{3-9}$$

It is esily shown that the slope dF_p/du at zero displacement is equal to $F_0\delta$. It is, thus, only dependent on velocity.
The damping force is accounted for by the dual term of Equation (3-2). This difference in behavior is due to the utilization of lower orifice area when stroke increases than when it decreases. Approximate expressions for the damping forces F_1 and F_2 are:

$$F_j = F_{\max j} \left[1 - \exp\left(-\varepsilon_j |\dot{u}|\right) \right] \ , \ j=1,2 \tag{3-10}$$

This expression was found to be appropriate for the tested device and for velocity up to about 500 mm/sec. A limitation of this expression is that it predicts constant damping force at large velocities, which is apparently incorrect. An alternative expression, which could account for the actual behavior at velocities beyond the range of testing is

$$F_1 = C_{11} |\dot{u}| \rightarrow |\dot{u}| \leq u_1 \tag{3-11a}$$

$$F_2 = C_{21} \dot{u}_1 + C_2 \left(|\dot{u}| - \dot{u}_1 \right)^{a_2} \rightarrow |\dot{u}| > \dot{u}_1 \tag{3-11b}$$

11

with $\dot{u}_1$ equal to about 50 mm/sec and a_j equal to about 0.3

The various parameters in the model of Equations (3-1) to (3-6) are illustrated in Figure 3-1. The calibrated parameters of the fluid device used herein are presented analytically in Section 3.
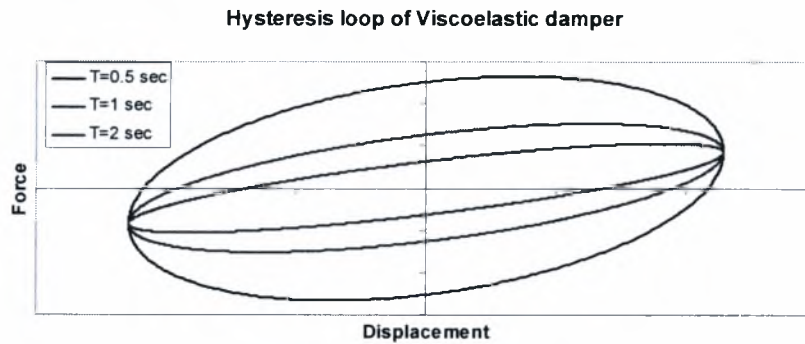
3.2   VISCOELASTIC DAMPERS

In this study a visco elastic damper was used to approximatelly account for the behavior of a fluid restoring force and damping device. Many types of viscoelastic devices and their corresponding mathematical models have been reported in the literature. In this work solid visco elastic devices are considered. These devices are similar to the one shown in the Figure 3-5 in construction. In general, the behavior of these dampers depends on frequency, strain ratio, and ambient temperature. The simplest mathematical model which has been proposed is the Kelvin model. It consists of a linear spring of stiffness K and a linear viscous dashpot with damping constant C. Figure 3-5 illustrates a viscoelastic damper.
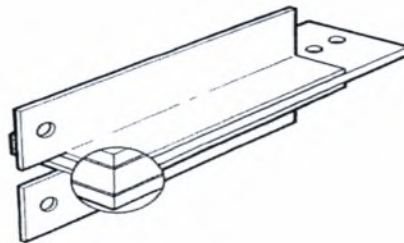
Figure 3-5 Viscoelastic Damper (Ramirez et.al 2001)

The values of K and C used in the analysis herein are these that used in Ramirez, as evaluated in the work of Constantinou. Further information about viscoelastic dampers may be found in the works of Zimmer (1999), Constantinou et al. (1998), Soong and Dargush (1997).

The experimental results have shown that the hysteresis loop of these devices has an elliptical shape. The area of this loop is the amount of energy that dissipated from the damper during a dynamic load. Figure 3-6 illustrates typical hysteresis loops of a viscoelastic damper. It can be easily observed the strong dependence of the visco elastic dampers to frequency. Even though such dampers are strongly influenced by temperature, this is not accounted for in this study since it is not within its scopus.

12

Hysteresis loop of Viscoelastic damper

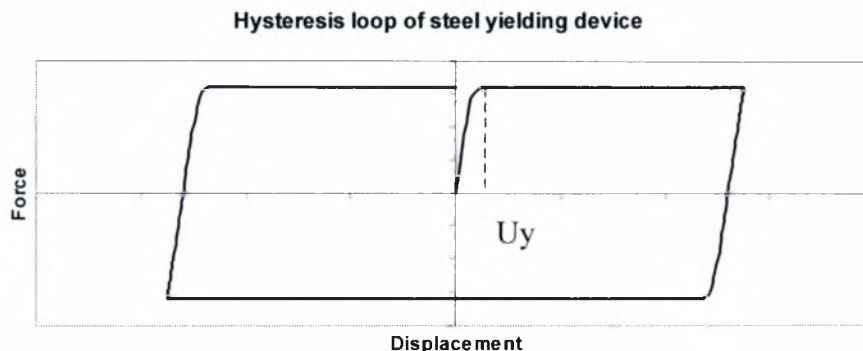**Figure 3-6 . Typical hysteresis loop of Viscoelastic device.**

3.3 METALLIC YIELDING DEVICES

Metallic yielding devices are also considered in the present work. More specifically, triangular plate steel damping devices as the one shown in Figure 3-7 are considered.
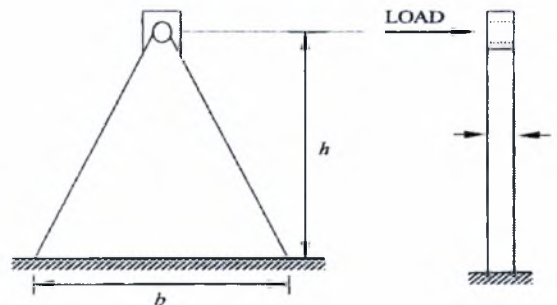
**Figure 3-7 . Triangular plate damping device (Ramirez et.al 2001)**

The geometry and the material properties as well as the design process of a structure with these devices is presented in Ramirez et al. (2002). The device has yielding stress and yielding strain which depend on the dimensions and the number of plates. The triangular shape ensures yielding over the entire height of the device. The hysteresis loop is elastoplastic, and the values need to describe it, is the yielding force and yielding displacement.

Hysteresis loop of steel yielding device

Figure 3- 8. Typical Hysteresis loop of Metallic Yielding Device

3.4 LINEAR VISCOUS DAMPERS

13

The linear viscous dampers provide the structure with added damping. The difference with the viscoelastic dampers is that linear viscous dampers do not have a stiffness component. These devices have a hysteresis loop with elliptical shape. To describe their behavior a dashpot with constant damping C is required. Their behavior is a function of frequency as depicted in Figure 3-9.
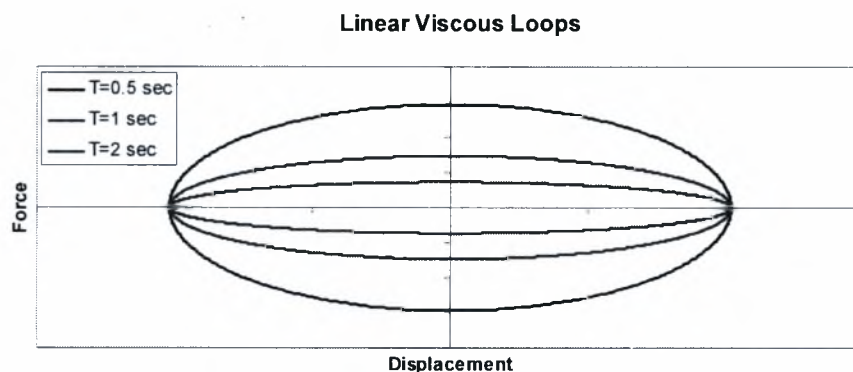
Figure 3- 9. Typical Hysteresis Loops of Linear Viscous Damper

3.5   EQUIVALENCY OF DAMPING SYSTEMS

The devices which are examined in the present study were presented. The objective of this work is to gain an insight on the influence of the constant restoring force in the dynamic response of multi story structures. This is objective is met through comparisons of the dynamic response of structural systems fitted with dampers/devices with constant restoring force to the dynamic response of the same structures fitted with other dampers/devices (e.g. visco-elastic, steel yielding, and fluid viscous). In order to have as clear view as possible, the devices, the one with the constant restoring force and its equivalent, are calibrated in a way that the energy absorbed, by both of them, per cycle of motion, as well as the maximum forces (if that is possible) are equal. That means for the same velocity and displacement time histories the areas of the force-displacement loops of the devices are equal and the maximum forces are comparable.

This equivalency is achieved by adjusting the damping force term of the fluid restoring force/damping device in the corresponding damping term of the comparable device. The damping force terms for all the considered devices are:

Viscoelastic and linear viscous: $F_D = C \cdot \dot{u}$ (3-12)

Steel yielding device: $F_D = F_y \cdot Z_D$ (3-13)

Fluid restoring force/damping device: $F_D = F_y \cdot \text{sgn} \, \dot{u}$ (3-14)

where C is damping coefficient, $\dot{u}$ is the velocity, F_y is the yielding force of the steel yielding damper, and Z_D is a dimensionless parameter described by the following equation:

14

$$u_{yd} \cdot Z_D + 0.5 \left| \dot{u} \right| Z_D \left| Z_D \right|^{\eta-1} + 0.5 \dot{u} \left| Z_D \right|^{\eta} - \dot{u} = 0 \tag{3-15}$$

The equations for the fluid restoring force and damping device were presented in detail in Section 3.1.

3.5.1 Effective Linear-Viscous and Visco-Elastic devices to the Fluid Restoring Force and Damping Devices.

To ensure that the linear viscus and the viscoelastic device give the same damping as the For the equivalency to the viscoelastic and linear viscous, the damping term of the fluid device is replaced by the linear term of Equation (3-12). Thus, practically exactly the same damping for the comparing devices is achieved.

The devices are excited by the same harmonic displacement and velocity time histories.

$$u = U_{max} \cdot \cos(\omega \cdot t) \tag{3-16}$$

$$v = \omega \cdot U_{max} \cdot \sin(\omega \cdot t) \tag{3-17}$$

$$\omega = 2\pi / T \tag{3-18}$$

The target of this process is that both the damping capacity (area under the force-displacement loop) and the maximum damping force, for the same displacement and velocity histories, are equivalent for the visco elastic or viscous devices and the constant restoring force devices. U_{max} in Equations (3-16) and (3-17), was selected to be the average maximum displacement of the dynamic response from the analysis of the structural model with the viscous damping devices. More specifically, nonlinear time history analyses were performed with the linear viscous dampers in the structural model under the suite of seismic motions considered in this study. The average of the maximum responses were calculated and were used to calibrate the parameters of the visco-elastic and the constant restoring force devices. For these U_{max} and for periods T= 0.5, 1, 2 sec, the force-displacement loops of the viscous and the visco-elastic dampers are illustrated in Figures 3-6 and 3-9. Then with the same data, we plot the hysteresis loops of the fluid device. Next the suitable values of constant restoring force must be selected.

The values of the constant restoring force, F_o, are critical for the structural response. These values should be such that they could not result in larger maximum damping forces than the maximum damping forces which are developed during the dynamic response of the building with the fluid viscous damping. Since the damping ratio C is constant, the values of the damping forces depend on the velocity, and in the case of the visco-elastic system, in addition, depend on displacements.

For the three aforementioned periods and for U_{max}= 125 mm the corresponding maximum damping forces for the harmonic velocity and displacement history for the

15

case of the visco-elastic damper (see Figure 3-10) are for T=0.5 sec F_D=1187 KN, for T=1 sec F_D=716 KN, and for =2 sec F_D=537 KN.

For periods 0.5 and 1 sec the velocities of the harmonic excitations are high when compared to the velocities experienced by the building during actual seismic excitations. Therefore the corresponding damping forces are unrealistic for the models that are examined herein. The maximum average damping force from the dynamic response of the structure with viscous dampers is 530 KN. Therefore, the parameter F_o of the FRFDD corresponding to the constant restoring force is chosen to be 75%, 50% and 25% of F_{max}, with F_{max}= 530 KN.

Hysteresis Loops of Viscoelastic system
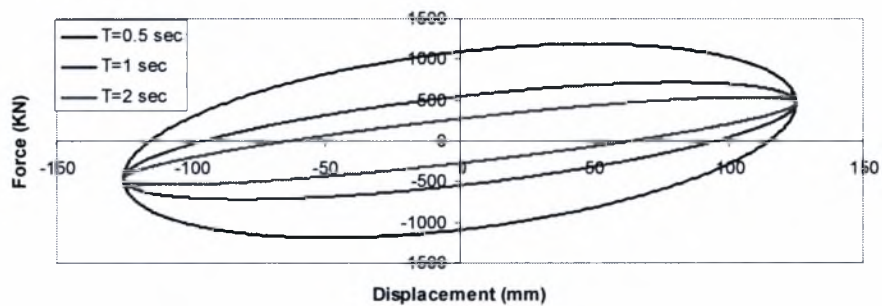
Figure 3-10 Force-Displacement loops of Viscoelastic dampers excited with harmonic displacements of T= 0.5, 1, and 2 sec and U_{max}= 125 mm.

In the following figure are plotted the hysteresis loops of the visco-elastic and the constant restoring force device, with F_0= 0.75*F_{max}= 397 KN and T=2 sec. Practically the area under the two loops is identical (the energy dissipated per cycle of motion is equal) but the way the devices respond is different (for the visco-elastic device the restoring force is proportional to displacements; for the FRFDD the restoring force is constant).

**Equivalent systems Viscoelastic - Fluid Device**
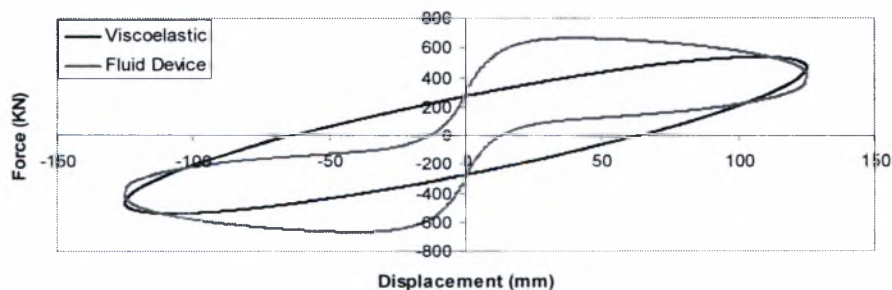
Figure 3-11 Hysteresis Loops of Visco-Elastic and Fluid Restoring Force and Damping Device (F_o= 0.75*F_{max}) for harmonic excitation of period T=2 sec and amplitude 125mm.
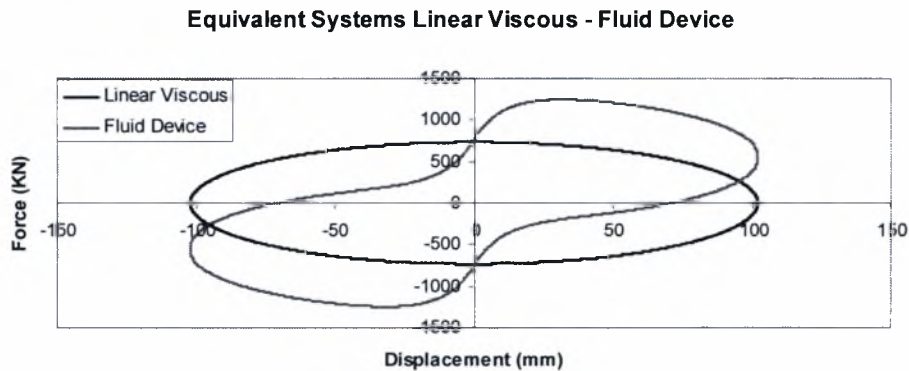
For linear viscous systems, following the same process (harmonic excitation with U_{max}= 102 mm, and T=0.5 sec F_D=2935 KN, and for T=1 sec F_D=1467 KN) the velocities are larger than the velocity response of the model. Again the appropriate values are for harmonic excitation with T=2 sec and U_{max}= 102 mm F_D=733 KN. The

16

forces of the linear viscous damper are larger than these of the other devices because the damping ratio is high enough, and these devices were used in the six story building.

For the period of 2 second, the maximum damping force is 733 KN, and the corresponding force from the dynamic response is 700. These are close enough and provide a good estimation for the equivalency. In Figure 3-13 are illustrated the equivalent hysteresis loops for the devices for period T=2 sec, $F_0=0.75*F_{max}=550$ KN and $U_{max}=102$ mm.

Hysteresis Loops of Linear Viscous Damper
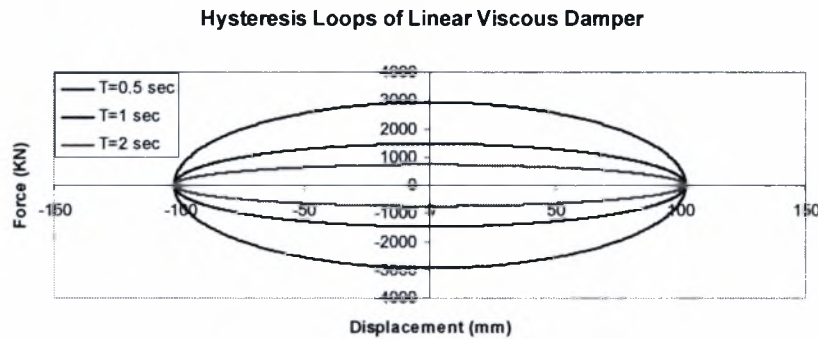
Figire 3-12 Hysteresis Loops for Linear Viscous System

Equivalent Systems Linear Viscous - Fluid Device

Figure 3-13 Hysteresis Loops of Linear Viscous and FRFD Device for period T=2 sec and $U_{max}= 102$ mm.

Again the areas of the loops are equal however the maximum forces of the FRFD device are larger from the equivalent devices as illustrated in the previous graphs. That happens because of the replaced damping term of the fluid device. With the replaced term is unbounded and the maximum value of the damping force is depented on the velocity and the restoring force. For smaller restoring force the corresponding damping force is smaller too.

3.5.2 Equivalency Metallic Yielding Device to FRFD Device

The structural model with the steel yielding dampers (see Section 4) is a 3- story building. The design requirements for that structure called for different damping force in each floor, $F_{D1}= 320 KN$ in the 1st floor, $F_{D2}= 240 KN$ in the 2nd floor, and

17

$F_{D3}= 187\ KN$ in the 3rd floor. Therefore for this study an equivalent FRFD device has to be calibrated for each floor.

The behavior of the metallic dampers/devices is independent of frequency and its maximum damping force (it is constant) is the yielding force. The maximum damping force of the FRFD device for motion away from neutral F_{max1} and for motion towards the neutral point is F_{max2}. The limits of the steel yielding damper force are F_{D1} and $-F_{D1}$. The constant restoring force of the FRFD device is F_o and has to always be smaller than F_{D1}, therefore the values of F_{max1} and F_{max2} have to be calibrated satisfying $F_{max1}= F_{D1} - F_o$ and $F_{max2}= F_{D1} + F_o$.

Figure 3-12 presents the force displacement loop of a FRFD device with these values and for $F_{D1}= 320$ KN and $U_{max}=150$ mm.

Hysteresis loop of fluid damper

Displacement (mm)
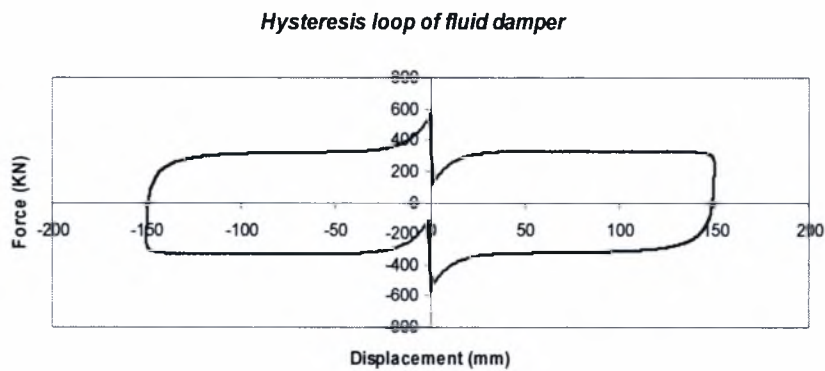
**Figure 3-14 Hysteresis loop of fluid damper for $F_{max1}= F_{D1} - F_0$ and $F_{max2}= F_{D1} + F_0$.**

It is clear from the Figure that the maximum force is not 320 KN in the vicinity of the neutral position. It is F_0+F_{max2}. Subsequently is described the process which was followed to overcome this discrepancy.

The restoring force depends on the displacement. For small displacements, F_o has not reach the maximum value. After a displacement threshold, F_o is constant at its maximum value. This is illustrated in Figure 3-13 where the slope is the stiffness of the device and is controlled from the variable δ_0 of Equation 3-9. The term F_{max2} is added to F_0 in the second and fourth quartile, Figure 3-14.

Constant Restoring Force of Fluid Device

Displacement (mm)
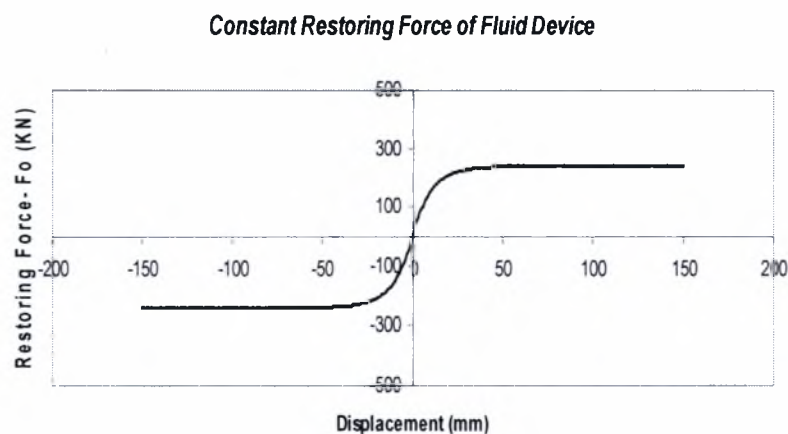
Figure 3-15 Constant Restoring Force- F_0 of Fluid Device

18
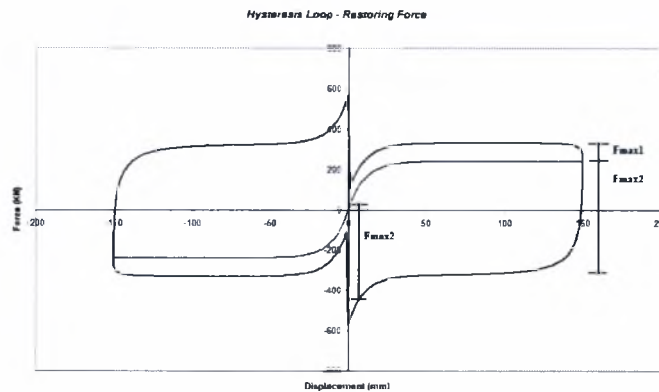
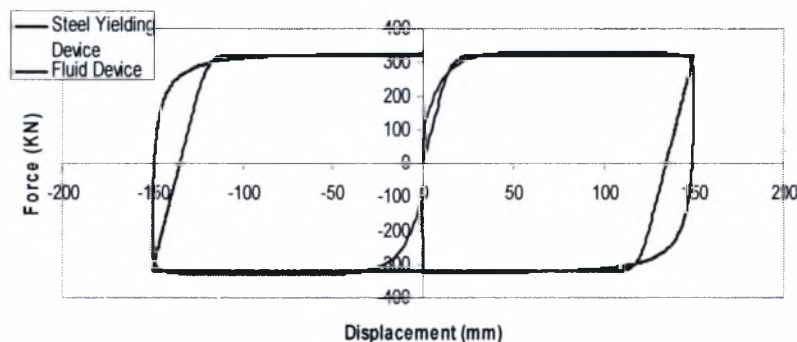**Figure 3-16 Hysteresis Loop- Restoring Force of Fluid Device**

This problem was solved by adjusting F_{max2}. From constant it is setted variable. At every point is added to the restoring force the value need to reach and not overcome the maximum force, ie the *X-distance + Constant Force F_{max2}* as shown in Figure 3-15.
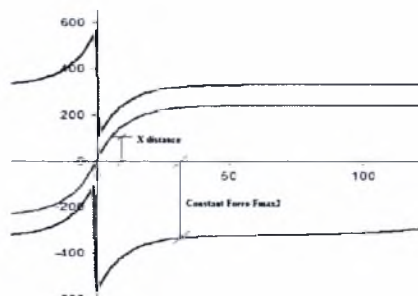
Figure 3-17 Graphical Definition of Variable Fmax2

With this definition of F_{max2} the equivalents fluid systems are constructed and we plot the equivalency graph of the first floor for U_{max}= 150 mm.

Figure 3-18 Hysteresis Loops for the 1ˢᵗ floor for Steel Yielding- Fluid Restoring Force and Damping Devices

19

4. ANALYTICAL MODELING

4.1   Introduction

In this section are presented mathematically the models that analyzed in the present study. In the work of Ramirez were analyzed buildings with energy dissipation systems. Adopted from the work of Ramirez et al. (2002), here 2 buildings were selected for the analyses, a 3-story, and a 6-story. The buildings firstly were designed and then analyzed inclusive the energy dissipation systems. The design of the dampers was presented in Ramirez et al (2002). The main characteristics and the data used for the analysis of the devices were presented in Section 3.

The designed buildings are illustrated in **Figure 4-1**. In this study the buildings were simulated as stick models with shear building type of behavior. The models are excited by far field and near field seismic motions.

As mentioned previously, three types of restoring force and damping devices are examined and their behavior is compared to the behavior of the same structural model with FRFD devices. The two buildings considered in this study are illustrated in **Figure 4-1**. In the parametric analyses the three types of devices, which their behavior is compared to the corresponding behavior of the FRFD devices, are utilized as follows within the two structural models:

- Model 1:   3- Story building with Visco-elastic devices
- Model 2:   3- Story building with Steel Yielding devices
- Model 3:   6- Story building with Linear Viscous devices

The buildings in Ramirez have three spans. Herein we made the equivalent shear model. For the shear model were calculated the equivalent stiffness, yielding force, yielding displacement and the post- yielding ratio.

The analyses follow the following steps:
STEP#1: The 3 models with the damping devices were analyzed.
STEP#2: The aforementioned models with FRFD devices were analyzed, with the effective parameters as were obtained in Section 3-5.

4.2   Non-Linear Time History Analysis

Non-linear time history analysis performed for each model by integrating the system of equations of motion with respect to time. The equation of motion is:

$$[M]\{\ddot{u}\} + [F_F] + [F_D] = [M]\{\ddot{u}_g\} \qquad (4\text{-}1)$$

Where, M is the mass matrix of the model, F_F is a matrix that describes the inelastic behaviour of the model and F_D is the damping force matrix that describes the behavior of the examined damping device. $\ddot{u}$ is the relative acceleration and $\ddot{u}_g$ is the ground acceleration. The solution of the differential equations is a vector $<u_i, \dot{u}_i, Z_{Fi}, Z_{Di}>$, where u_i is the relative displacement, $\dot{u}_i$ is the relative velocity, Z_{Fi} and Z_{Di} are

20

dimensionless parameters for the building force and the damper's force respectively, and i=1, 2,...,n where n is the number of the model's floors. The relative acceleration is calculated by Equation 4-1 with the vectors known.

4.2.1 Description of the Building Behavior

The behavior of the models is smooth perfect bilinear and is described with the following equations:

$$F_F = \alpha \frac{F_y}{D_y} u + (1-\alpha) F_y Z_F \tag{4-2}$$

$$D_y \dot{Z}_F + 0.5 |\dot{u}| Z_F |Z_F|^{\eta-1} + 0.5 \dot{u} |Z_F|^{\eta} - \dot{u} = 0 \tag{4-3}$$

D_y is the yielding displacement of the model, F_y the yielding force, α is the pre-yielding to post yielding stiffness ratio, Z_F is a dimensionless parameter described by the differential Equation 4-3, and η is a dimensionless parameter that controls the smoothness of the transition from elastic to inelastic area, **Figure 4-4.**

4.2.2 Description of Devices

The behavior of the devices is described by the hysteresis loops that presented in the previous section. F_D is the damper's force, and the following expressions were used for the analysis:

- *Viscoelastic*

$$F_D = Ku + C\dot{u} \tag{4-4}$$

- *Linear Viscous*

$$F_D = C\dot{u} \tag{4-5}$$

- *Steel Yielding*

$$F_D = F_d Z_D \tag{4-6}$$

$$D_{yd}\dot{Z}_D + 0.5 |\dot{u}| Z_D |Z_D|^{\eta-1} + 0.5 \dot{u} |Z_D|^{\eta-1} - \dot{u} = 0 \tag{4-7}$$

$\dot{u}$, u are the relative velocity and relative displacement, K and C are the stiffness and the damping ratio of the damper with constant values. F_d, D_{yd} are the yielding force and displacement of the device respectively, Z_D is a dimensionless parameter described by the differential equation 4-7. For these three cases was performed non-linear time history analysis. The results are presented in the next section.

21

4.2.3 Description of Fluid Device

The general equation describing the behavior of the fluid device is Equation (3-6):

$$F_t = F_0 \left[1 - \exp(-\delta|u|) \right] \mathrm{sgn}(u) + K_0 u + \left[F_{min} + \zeta K_0 |u| \right] Z_t + F_d \, \mathrm{sgn}(\dot{u})$$

In the previous sections were explained and presented the changes that made in the model in order to have equivalent systems, so that the results could be comparable and the influence of the constant restoring is more clear. Analytically used the next mathematically expressions:

- *For equivalent system to Linear Viscous and Viscoelastic*

$$F_D = F_0 \left[1 - \exp(-\delta|u|) \right] \mathrm{sgn}(u) + K_0 u + \left[F_{min} + \zeta K_0 |u| \right] Z_t + C \dot{u} \, \mathrm{sgn}(\dot{u}) \qquad (4\text{-}8)$$

- *For equivalent system to Steel Yielding*

$$F_D = F_0 \left[1 - \exp(-\delta|u|) \right] \mathrm{sgn}(u) + K_0 u + \left[F_{min} + \zeta K_0 |u| \right] Z_t + F_d \, \mathrm{sgn}(\dot{u}) \qquad (4\text{-}9)$$

where for $u \dot{u} > 0$

$$F_d = F_{max1} \left(1 - \exp\left(-e1|u| \right) \right) \qquad (4\text{-}10)$$

for $u \dot{u} < 0$

$$F_d = \left| F_0 \, \mathrm{sgn}(u)(1 - \exp(-\delta|u|)) + F_{max2} \, \mathrm{sgn}(u) \right| \cdot (1 - \exp(-e2|u|)) \qquad (4\text{-}11)$$
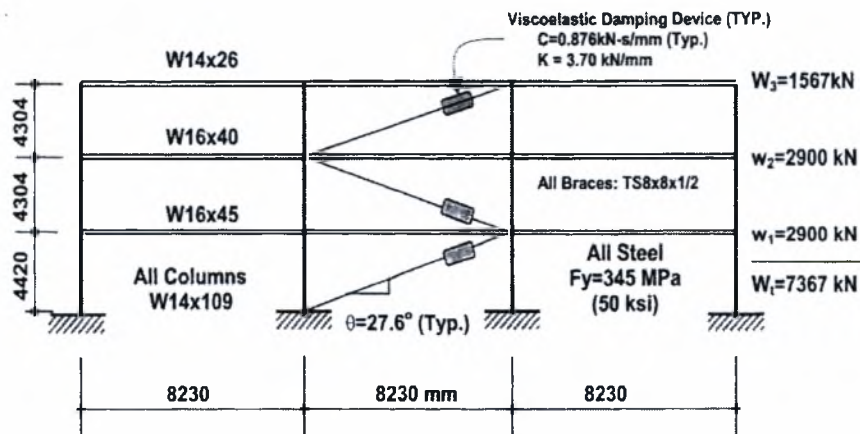
Figure 4.1(a) 3- story building equipped with viscoelastic dampers (from Ramirez et al. 2002)

22
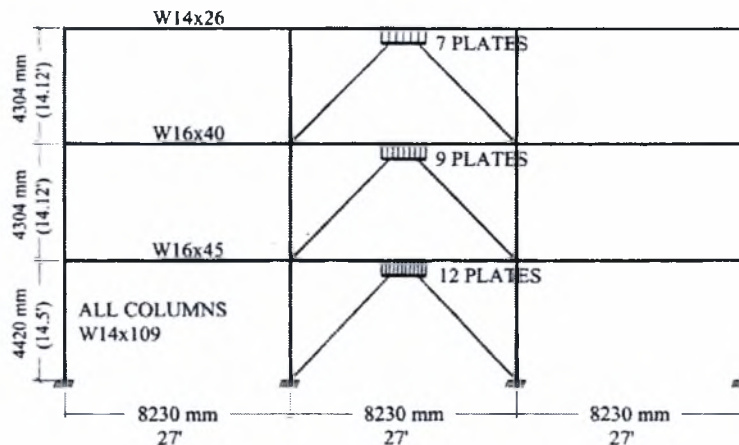
Figure 4.1(b) 3- story building equipped with steel yielding dampers (from Ramirez et al. 2002)
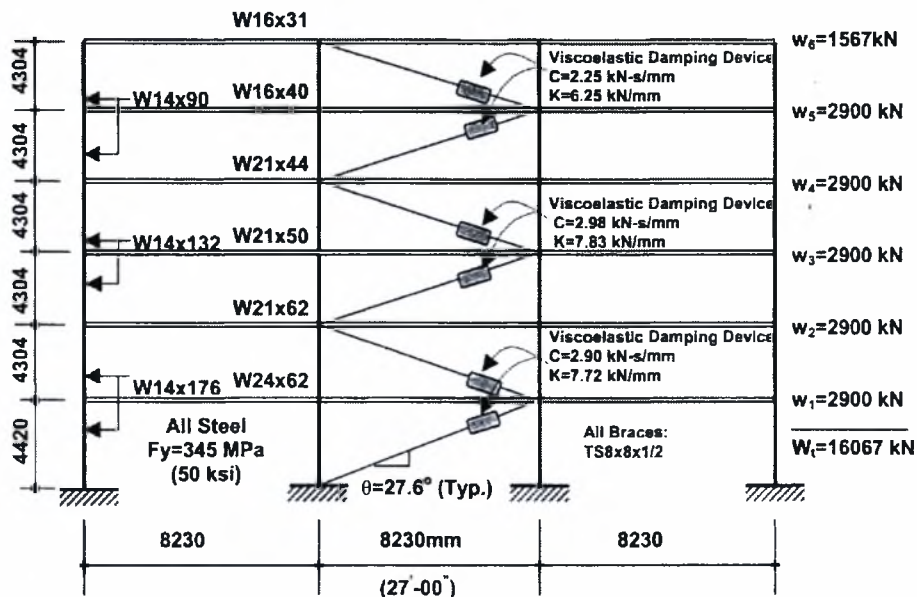
Figure 4.1(c) 6- story building equipped with linear viscous dampers
Figure 4.1 The buildings that examined in this study equipped with damping devices (from Ramirez et al. 2002)
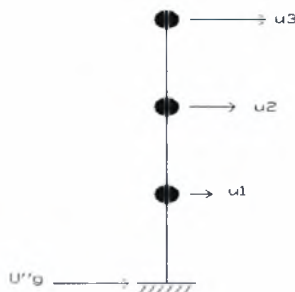

Figure 4-2 Three story shear model with one degree of freedom, displacement at X-axis.

23

4.2.4 Design of steel moment frames.

The steel moments frames designed to meet NEHRP (1997) criteria without damping systems. The designed frames are presented in the next figures.
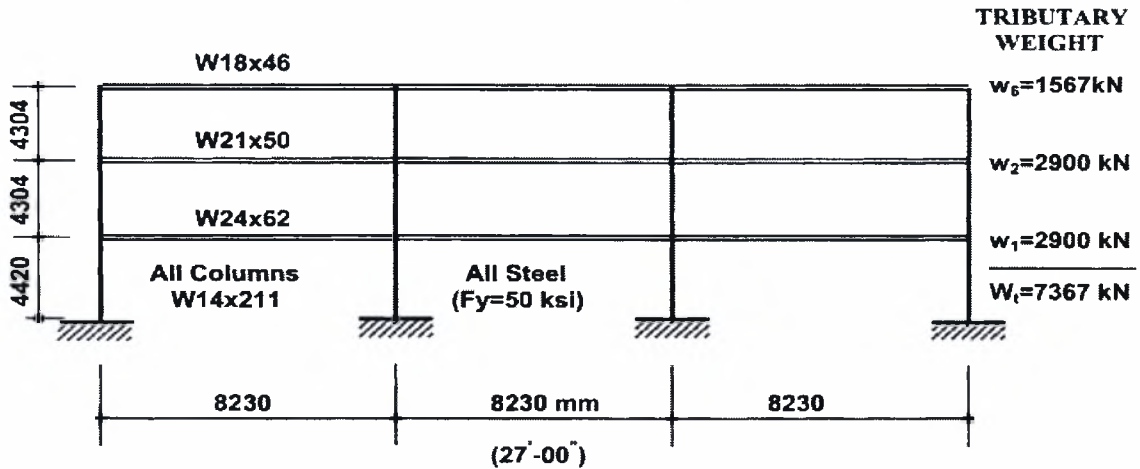
Figure 4.3(a) 3-Story Special Steel Moment Frame Designed to Meet NEHRP (1997) Criteria without a Damping System (Ramirez 2002).
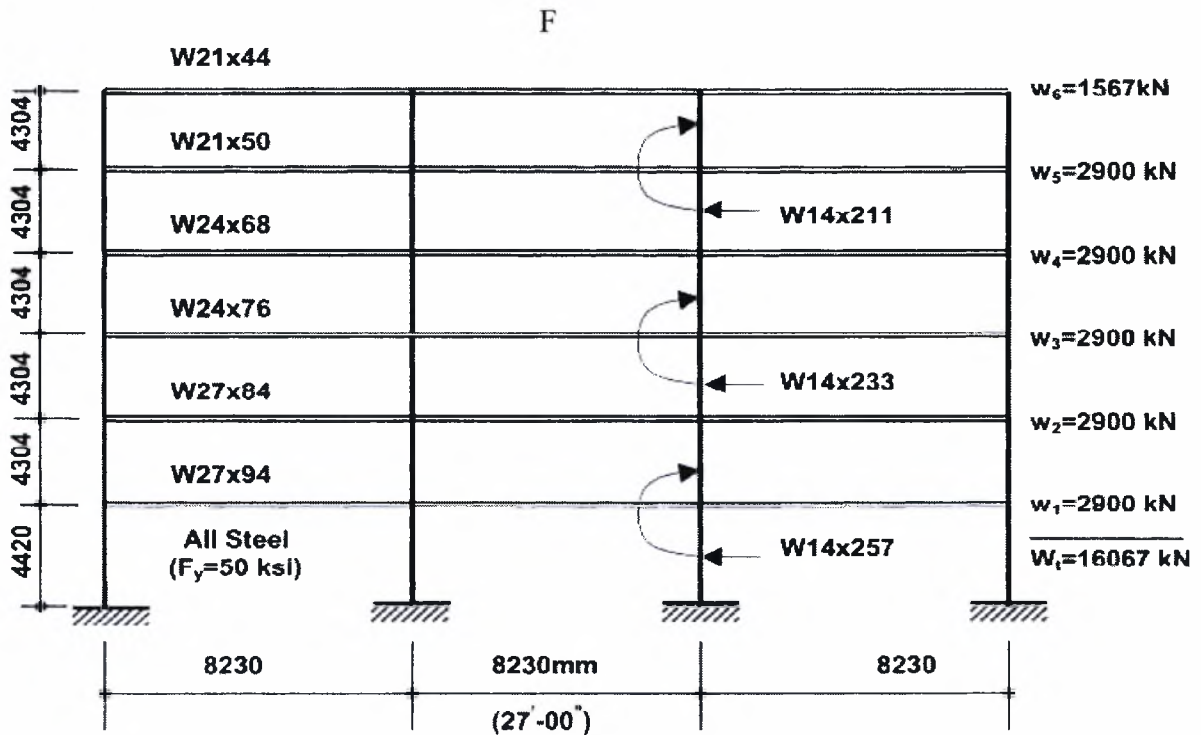
Figure 4.3(b) 6-Story Special Steel Moment Frame Designed to Meet NEHRP (1997) Criteria without a Damping System (Ramirez 2002).
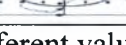
24

5. SUMMARY OF THE RESULTS AND CONCLUSIONS

The results from the nonlinear time history analysis are tabulated in this section. Each table contains the maximum parameter (interstory drift, floor acceleration, velocity, shear force, and damper force) at every floor of the model and for all the ground excitations considered in the particular analysis. The PGA for each seismic excitation are indicated in the top row of each table.

The analyses are divided in three groups. In the first and second group (indicated as Model 1 and Model 2 below), the 3-story structural model presented in a previous section is utilized. In the third group (indicated as Model 3 below)the 6-story structural model, also presented in a previous section is utilized. and the Following the analysis cases are presented with graph of the hysteresis loop. First with the letter A are described the far field motions, B for the near field and with the numbers the models as presented in the previous section. Thus:

TABLE 5-1

		Structural Model	Energy Dissipation System
MODEL 1	CASE A1-1	3-Story	Visco-elastic Damper
	CASE A1-2		Fluid Restoring Force/Damping Device $F_0=0.75 \cdot F_{max}$
	CASE A1-3		FRFDD $F_0=0.5 \cdot F_{max}$
	CASE A1-4		FRFDD $F_0=0.25 \cdot F_{max}$
MODEL 2	CASE A2-1	3-Story	Steel Yielding Damper
	CASE A2-2		FRFDD $F_0=0.75 \cdot F_{max}$
	CASE A2-3		FRFDD $F_0=0.5 \cdot F_{max}$
	CASE A2-4		FRFDD $F_0=0.25 \cdot F_{max}$
	CASE A2-5		FRFDD $F_0=0.75 \cdot F_{max}$
	CASE A2-6		FRFDD $F_0=0.75 \cdot F_{max}$
MODEL 3	CASE A3-1	6-Story	Linear Viscous Damper
	CASE A3-2		FRFDD $F_0=0.75 \cdot F_{max}$
	CASE A3-3		FRFDD $F_0=0.5 \cdot F_{max}$
	CASE A3-4		FRFDD $F_0=0.25 \cdot F_{max}$
	CASE A3-5		FRFDD $F_0=0.75 \cdot F_{max}$ (different value at every 2 floors)
	CASE A3-6		FRFDD $F_0=0.75 \cdot F_{max}$
	CASE A3-7		FRFDD $F_0=0.75 \cdot F_{max}$

25
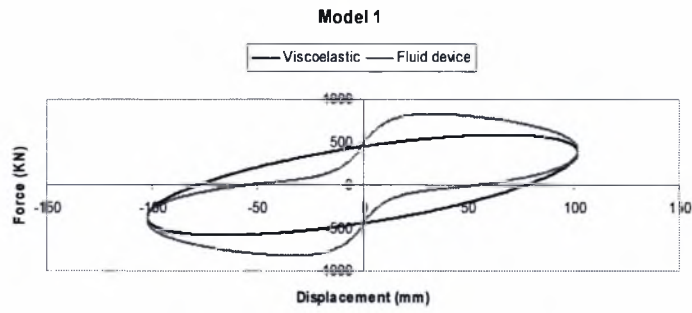
Model 1

Figure 5-1. Hysteresis loops of model 1, Visco-elastic and the equivalent Fluid device for cases 1-1 to 1-4.
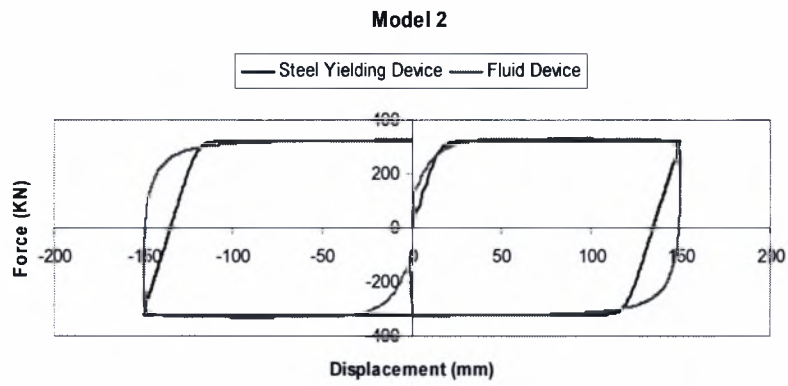
Model 2

Figure 5-2. Hysteresis loops of model 2, Steel Yielding and the equivalent Fluid device for cases 2-1 to 2-4.

26

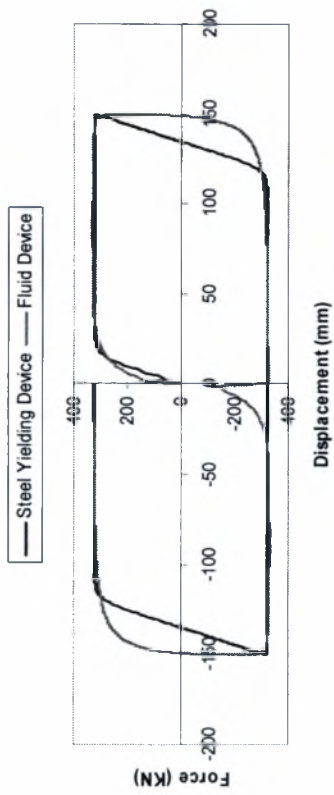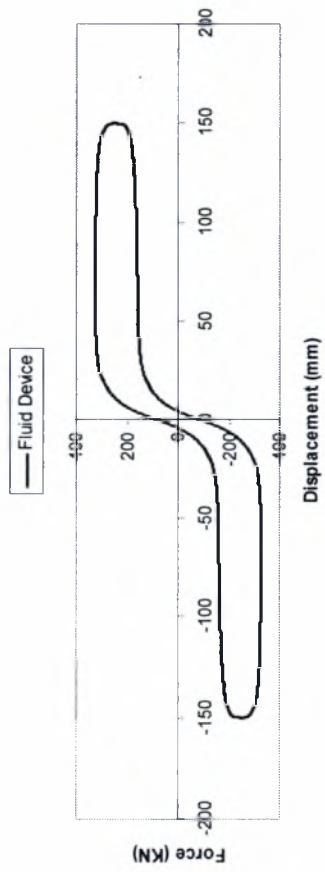**Figure 2. Hysteresis loops of model 2, Steel Yielding and the equivalent Fluid device for cases 2-1 to 2-4**

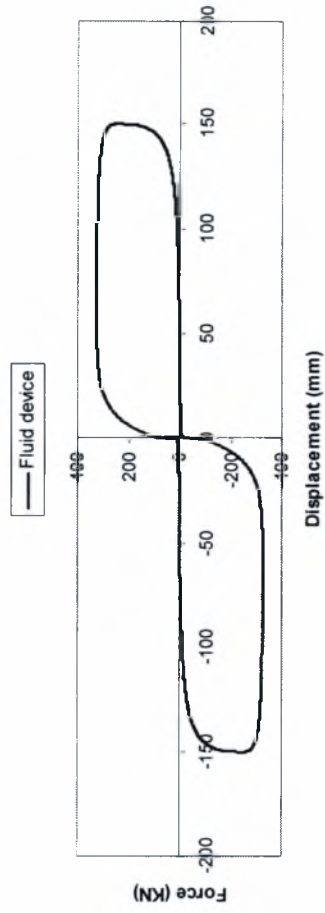

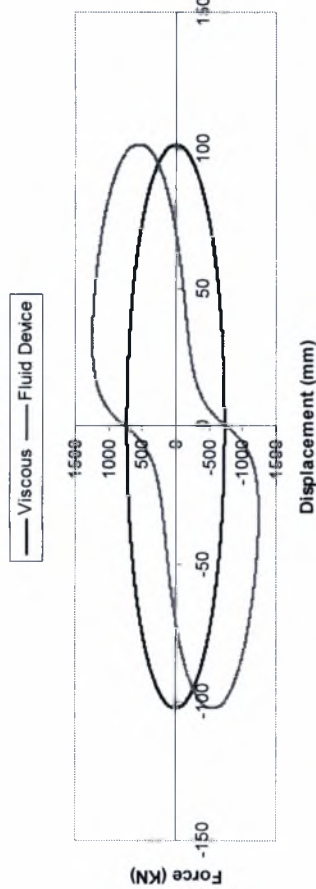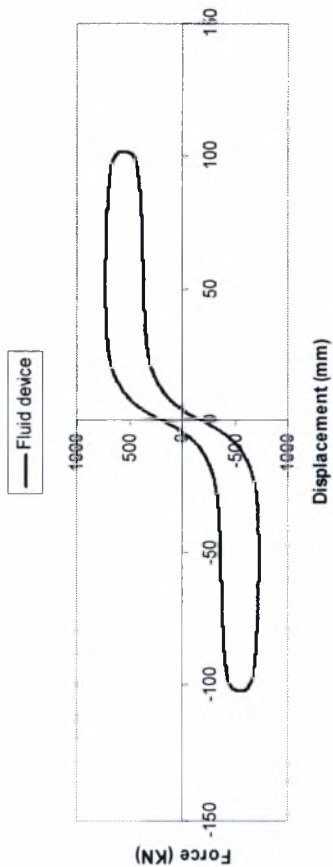**Figure 3. Hysteresis loop of Fluid device for case 2-5.**

Figure 4. Hysteresis loop of Fluid device for case 2-6.

27

Model 3
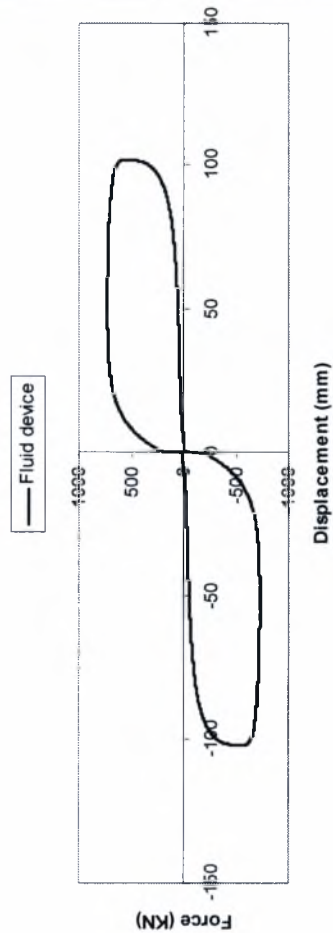
Figure 5. Hysteresis loop for Model 3 for Viscous and the equivalent Fluid device for cases 3-1 to 3-5.

Model 3

Figure 6. Hysteresis loop of Fluid device for case 3-7.

Model 3

Figure 7. Hysteresis loop of Fluid device for case 3-8.

28

TABLE 5-2 Average response parameters from nonlinear time history analyses of the 3-story structure excited with Far-Field motions (MODEL 1)

CASE	FLOOR	Interstory Drift (mm)	Interstory Velocity (mm/sec)	Acceleration (g)	Shear Force (kN)	Damper Force (kN)
CASE A1-1	3	15.9	134.7	0.348	551.0	114.5
	2	46.1	278.1	0.238	1116.8	244.8
	1	124.7	489.5	0.264	1490.8	530.9
CASE A1-2 $F_0=397$ KN	3	10	102.3	0.368	582.7	285.7
	2	33.2	243.0	0.271	1299.4	502.3
	1	112.6	489.6	0.298	1643.2	705.2
CASE A1-3 $F_0=265$ KN	3	11.4	107.6	0.351	555.2	222.3
	2	36.4	250.4	0.248	1201.8	393.4
	1	123.4	480.9	0.284	1516.9	576.9
CASE A1-4 $F_0=132,5$ KN	3	13.2	113.9	0.330	522.6	152.1
	2	41.2	259.9	0.226	1098.3	283.6
	1	137.9	487.5	0.263	1392.6	451.1

29

TABLE 5-3 Average response parameters from nonlinear time history analyses of the 3-story structure excited with Far-Field motions (MODEL 2)

CASE	FLOOR	Interstory Drift (mm)	Interstory Velocity (mm/sec)	Acceleration (g)	Shear Force (kN)	Damper Force (kN)
CASE A2-1	3	21.8	307.6	0.528	835.2	181.6
	2	49.1	355.7	0.341	1186.9	240.2
	1	148.4	498.2	0.406	1321.5	321.3
CASE A2-2 F0=0.75 Fmax	3	14.2	115.0	0.350	553.7	124.1
	2	41.2	261.0	0.225	1117.6	221.1
	1	144.3	496.5	0.248	1303.5	324.7
CASE A2-3 F0=0.5 Fmax	3	14.3	111.9	0.333	527.4	109.6
	2	42.7	258.4	0.218	1086.9	208.7
	1	143.9	492.6	0.241	1287.8	316.5
CASE A2-4 F0=0.25 Fmax	3	14.6	111.0	0.321	507.6	101.3
	2	44.0	255.9	0.214	1062.5	200.4
	1	143.7	488.0	0.235	1274.4	309.3
CASE A2-5 F0=0.75 Fmax	3	17.4	192.9	0.417	659.4	139.3
	2	47.7	334.0	0.256	1147.7	226.4
	1	158.4	580.3	0.352	1314.3	326.5
CASE A2-6 F0=0.75 Fmax	3	15.6	146.4	0.379	600.0	130.8
	2	44.0	294.4	0.232	1129.6	223.0
	1	153.3	544.3	0.289	1309.5	325.6

30

TABLE 5-4 Average response parameters from nonlinear time history analyses of the 6story structure excited with Far-Field motions (MODEL 3)

CASE	FLOOR	Interstory Drift (mm)	Interstory Velocity (mm/sec)	Acceleration (g)	Shear Force (kN)	Damper Force (kN)
CASE A3-1	6	8.5	44.8	0.177	78.457	280.44
	5	22.4	110.7	0.149	193.73	710.3
	4	35.1	143.9	0.112	307.9	968.47
	3	54.5	173.3	0.125	370.91	1112.7
	2	74.1	209.9	0.162	480.61	1243.1
	1	102.1	305.4	0.233	699.46	1491.4
CASE A3-2	6	4.7	38.8	0.240	242.01	379.68
	5	16.2	101.7	0.212	539.07	987.04
	4	27.7	146.2	0.166	720.03	1397.5
	3	42.5	192.3	0.176	810.66	1636.5
	2	64.5	247.2	0.220	945.78	1843.3
	1	98.3	383.6	0.274	1262.6	2167
CASE A3-3	6	5.4	39.1	0.217	188.41	343.09
	5	17.6	103.8	0.189	416.02	887.58
	4	28.9	147.0	0.147	566.95	1237
	3	45.4	184.9	0.159	643.3	1450
	2	65.9	231.1	0.199	750.37	1635.9
	1	99.4	355.9	0.258	1038.7	1945.9
CASE A3-4	6	6.5	40.4	0.195	130.82	308.16
	5	19.6	106.3	0.168	294.42	791.86
	4	31.9	141.9	0.128	420.78	1101.6
	3	49.6	177.0	0.141	478.75	1291.2
	2	69.3	221.8	0.177	574.41	1441
	1	98.4	323.4	0.244	815.36	1703.7

31

TABLE 5-4 (continue) Average response parameters from nonlinear time history analyses of the 6story structure excited with Far-Field motions (MODEL 3)

CASE	FLOOR	Interstory Drift (mm)	Interstory Velocity (mm/sec)	Acceleration (g)	Shear Force (kN)	Damper Force (kN)
CASE A3-5	6	10.0	63.3	0.248	144.73	391.89
	5	28.7	162.7	0.200	337.65	966.84
	4	37.0	174.1	0.165	549.38	1296
	3	64.1	241.7	0.188	645.12	1517.5
	2	53.2	224.5	0.243	882.63	1747.8
	1	86.5	342.1	0.282	1168.5	2061.1
CASE A3-6	6	6.2	70.5	0.298	284.14	470.36
	5	20.2	178.1	0.236	534.52	1124.2
	4	32.6	209.9	0.197	601.12	1425.5
	3	44.8	237.2	0.245	630.18	1540
	2	63.1	285.3	0.306	648.68	1603.1
	1	169.9	596.2	0.335	695.1	1685.9
CASE A3-7	6	5.2	43.7	0.259	250.36	408.76
	5	17.8	119.8	0.221	505.84	1033.7
	4	29.3	167.8	0.161	588.12	1371
	3	41.3	196.0	0.186	619.2	1511.3
	2	57.9	252.5	0.236	641.49	1590.3
	1	160.9	536.8	0.275	692.63	1677.3

32

TABLE 5-5 Average response parameters from nonlinear time history analyses of the 3-story structure excited with Near-Faultmotions (MODEL 1)

CASE	FLOOR	Interstory Drift (mm)	Interstory Velocity (mm/sec)	Acceleration (g)	Shear Force (kN)	Damper Force (kN)
CASE B1-1	3	15.8	142.0	0.346	546.428	117.058
	2	60.8	291.6	0.251	1136.278	270.055
	1	161.5	541.7	0.270	1594.820	640.460
CASE B1-2	3	8.9	93.7	0.366	578.400	312.003
	2	33.1	239.3	0.287	1328.839	560.083
	1	170.7	572.8	0.306	1753.843	842.050
CASE B1-3	3	10.5	100.1	0.348	550.073	242.541
	2	36.9	248.3	0.261	1214.188	426.775
	1	178.9	567.8	0.273	1605.608	684.716
CASE B1-4	3	12.5	109.2	0.326	515.906	162.349
	2	42.3	257.5	0.232	1091.484	295.318
	1	186.5	554.4	0.247	1445.234	523.876

33

TABLE 5-6 Average response parameters from nonlinear time history analyses of the 3-story structure excited with Near-Faultmotions (MODEL 2)

CASE	FLOOR	Interstory Drift (mm)	Interstory Velocity (mm/sec)	Acceleration (g)	Shear Force (kN)	Damper Force (kN)
CASE B2-1	3	19.4	252.2	0.477	754.538	173.502
	2	47.5	335.1	0.167	1157.418	239.960
	1	221.1	626.5	0.311	1345.316	321.257
CASE B2-2	3	13.9	113.9	0.342	539.930	119.909
	2	39.4	257.3	0.221	1077.314	215.483
	1	209.7	585.9	0.243	1301.631	316.482
CASE B2-3	3	14.1	113.3	0.326	515.215	105.907
	2	40.2	256.9	0.212	1042.815	200.433
	1	210.6	577.8	0.236	1277.859	305.124
CASE B2-4	3	14.3	113.3	0.313	494.626	98.059
	2	41.8	257.4	0.206	1015.374	190.925
	1	212.3	570.9	0.231	1259.594	296.532
CASE B2-5	3	15.6	145.3	0.377	595.329	128.662
	2	44.5	295.8	0.235	1105.198	219.977
	1	238.1	668.9	0.298	1332.119	318.943
CASE B2-6	3	14.6	124.6	0.357	563.785	123.990
	2	41.5	277.2	0.226	1088.173	217.420
	1	226.7	634.5	0.272	1316.775	317.646

34

TABLE 5-7 Average response parameters from nonlinear time history analyses of the 6-story structure excited with Near-Fault motions (MODEL 3)

CASE	FLOOR	Interstory Drift (mm)	Interstory Velocity (mm/sec)	Acceleration (g)	Shear Force (kN)	Damper Force (kN)
CASE B3-1	6	8.9	47.5	0.187	295.006	83.200
	5	23.4	117.9	0.152	731.850	206.396
	4	42.2	154.6	0.123	978.458	330.948
	3	88.6	187.0	0.137	1168.931	400.224
	2	139.1	249.7	0.176	1405.066	571.752
	1	202.2	400.3	0.244	1763.988	916.606
CASE B3-2	6	4.5	36.8	0.231	365.731	232.495
	5	15.7	97.0	0.204	953.356	518.964
	4	28.3	144.5	0.165	1349.763	693.188
	3	58.6	197.4	0.174	1613.406	806.809
	2	112.3	280.4	0.215	1895.115	1025.984
	1	186.7	452.6	0.283	2325.649	1465.931
CASE B3-3	6	5.4	38.3	0.216	341.054	187.156
	5	17.6	102.3	0.186	879.157	412.568
	4	31.1	149.8	0.149	1227.142	557.588
	3	67.4	196.0	0.162	1465.893	656.013
	2	123.3	265.9	0.202	1739.820	866.946
	1	197.3	424.4	0.266	2121.263	1245.560
CASE B3-4	6	6.7	40.7	0.199	314.619	133.969
	5	19.9	107.6	0.167	798.752	301.750
	4	35.3	151.5	0.135	1095.749	425.254
	3	78.3	192.0	0.146	1322.487	503.171
	2	133.2	253.4	0.184	1574.194	707.722
	1	203.0	404.9	0.250	1932.513	1056.823

35

TABLE 5-7 (continue) Average response parameters from nonlinear time history analyses of the 6-story structure excited with Near-Fault motions (MODEL 3)

CASE	FLOOR	Interstory Drift (mm)	Interstory Velocity (mm/sec)	Acceleration (g)	Shear Force (kN)	Damper Force (kN)
CASE B3-5	6	9.5	60.3	0.237	374.360	139.069
	5	27.8	154.6	0.191	922.841	323.072
	4	41.1	168.9	0.161	1249.237	527.008
	3	95.1	234.8	0.187	1509.975	661.500
	2	100.9	240.5	0.240	1815.906	967.644
	1	176.0	422.9	0.285	2259.330	1400.023
CASE B3-6	6	5.9	59.1	0.284	448.889	271.384
	5	19.6	149.4	0.226	1082.396	517.474
	4	31.4	201.1	0.185	1364.654	586.063
	3	59.6	270.6	0.245	1482.635	610.704
	2	119.9	351.3	0.304	1581.225	637.936
	1	407.2	778.1	0.362	1776.181	683.862
CASE B3-7	6	5.0	40.8	0.251	397.485	243.555
	5	17.3	111.4	0.212	1000.085	491.081
	4	28.3	162.2	0.155	1316.779	572.129
	3	50.8	214.0	0.183	1446.160	601.381
	2	106.4	274.2	0.226	1556.452	628.468
	1	389.2	720.6	0.285	1749.888	679.650

36

37

5.1 CONCLUSIONS AND RECOMMENDATIONS

Previously, the response of three models equipped with damping devices and the equivalent fluid/ constant restoring force systems under near-field and far-field seismic excitations was examined in detail.

The influence of the constant restoring force is beneficial comparing with the other devices, when the constant restoring force has a value 50% or larger of the maximum force of the compared device. Generally, a high value of constant restoring force, mitigates the displacement response of the structure, the displacement of the first floor is slightly reduced, but a significant reduction is presented in the drifts between the floors, sometimes even in the level of 50%, comparing with the response of the other dampers. The reduction is proportional to the value of the constant restoring force. Moreover the permanent displacements are reduced significantly.

The presence of the constant restoring force results in increased accelerations and shear forces. By adding damping this problem is overcomed and the accelerations are reduced. Another worth mentioning result that is observed for all the response quantities, is that although the peak response value maybe the same or even larger for the fluid device, at the rest of the time history, the values are significant lower until the motion is finished, this can be clear from the plotted time histories. For the 3-story model, the constant restoring force mitigates the displacements and the added damping mitigates the accelerations, without affecting the displacements significant. But for the 6-story model, the added damping is extremely effective in the reduction of the displacement. Hence, a high value of constant restoring force with the appropriate added damping, leads to an improved dynamic response and an attractive design may achieved.

5.2 Comparing Results of the analysis
Comparing results of Viscoelastic Device – Fluid Device

Figures (6-1) to(6-8) present the results of floor displacements, velocities, accelerations and shear forces of the 3-story structure with the viscoelastic devices and the three designs of FRFDD devices. It is clear from these figures that the presence of constant restoring force is beneficial when it takes values larger than half of the maximum viscoelastic force. For these values the displacement response is better, and there is a great reduction in the drifts

For the 3-story structure, figure (6-9) to (6-17) compare the results between the steel yielding dampers and their equivalent FRFDD devices. The steel yielding device results in large accelerations, but for the equivalent cases of the fluid device are significantly reducted. The shear forces are proportional to the response of the displacements, large mitigation of displacement result in proportional mitigation of the shear forces.

Figures (6-18) to (6-24) compare the results for a 6-story structure with fluid viscous dampers and FRFDD devices. For model 3, as previous, the fluid device presents the same mitigation for the displacement response. Although the reduction of the displacements is satisfactory, important increasing in the shear forces occurs. This undesirable increasement is not reduced by adding damping. Totally the response for this model is not as satisfactory as for the models 1 and 2 where the shear forces are kept in satisfactory levels.

38

Results of model 1 for far field motions.
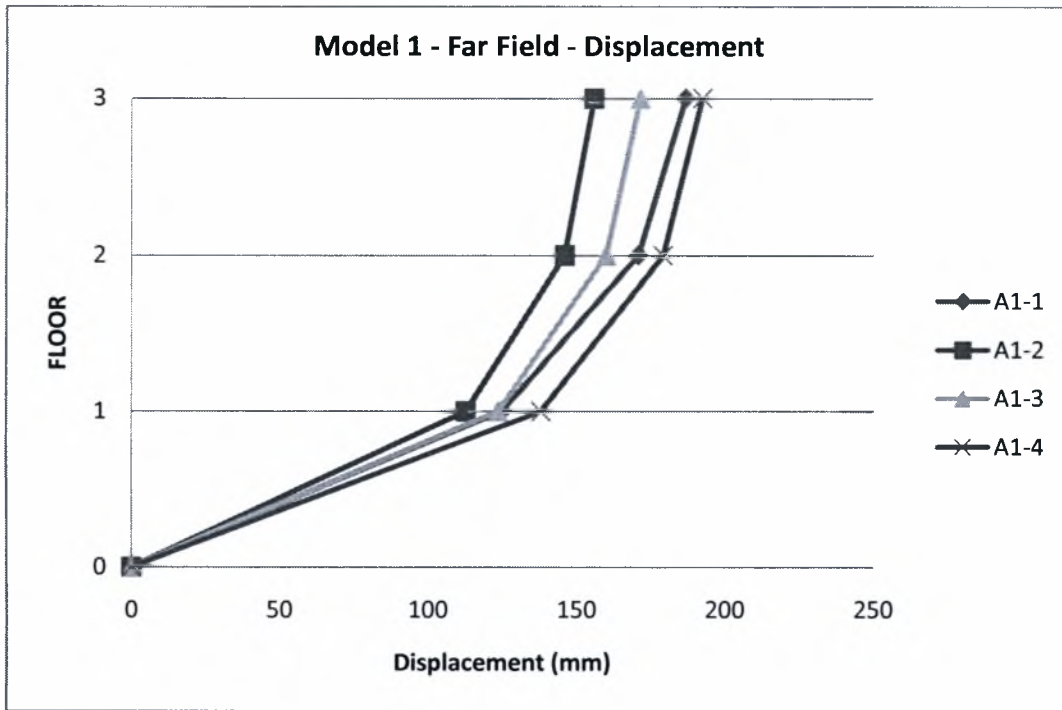
Figure 6-1 Displacements of Model 1 for Far-Field motions.
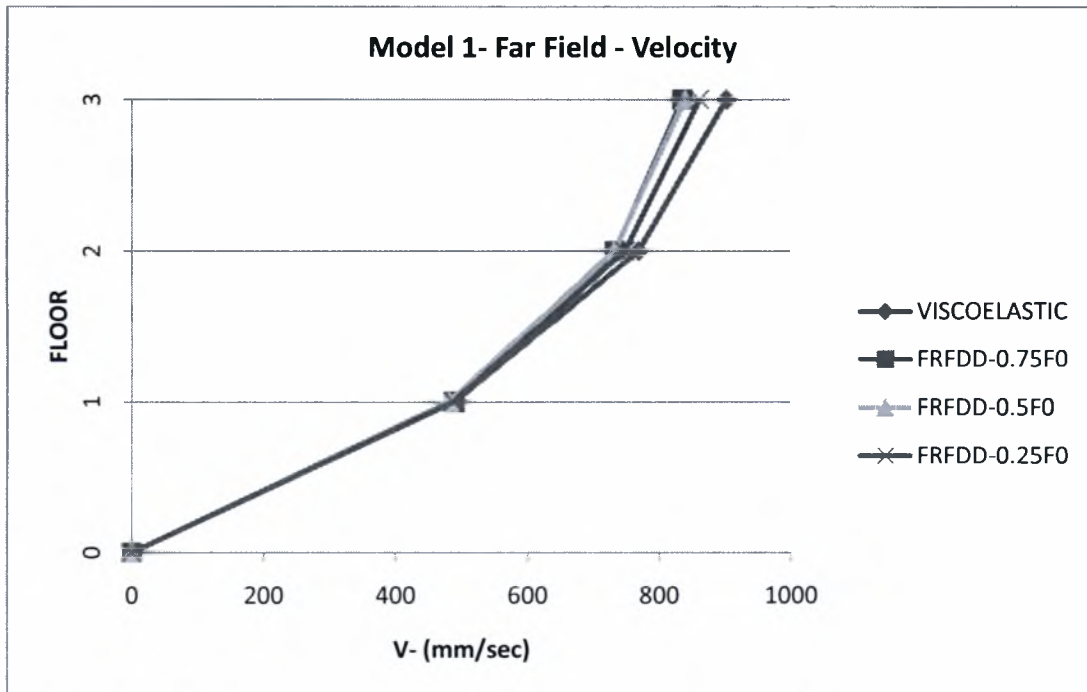
Figure 6-2 Velocity of Model 1 for Far field motions.

39
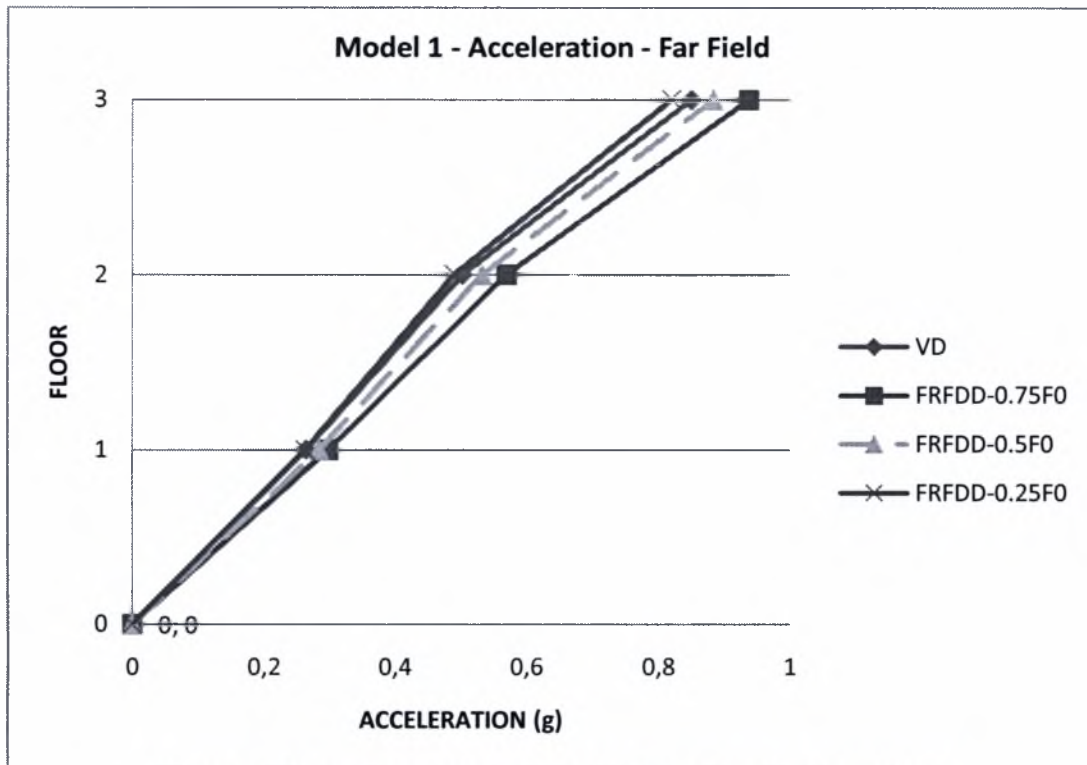
Figure 6-3 Accelerations of Model 2 for Far Field motions
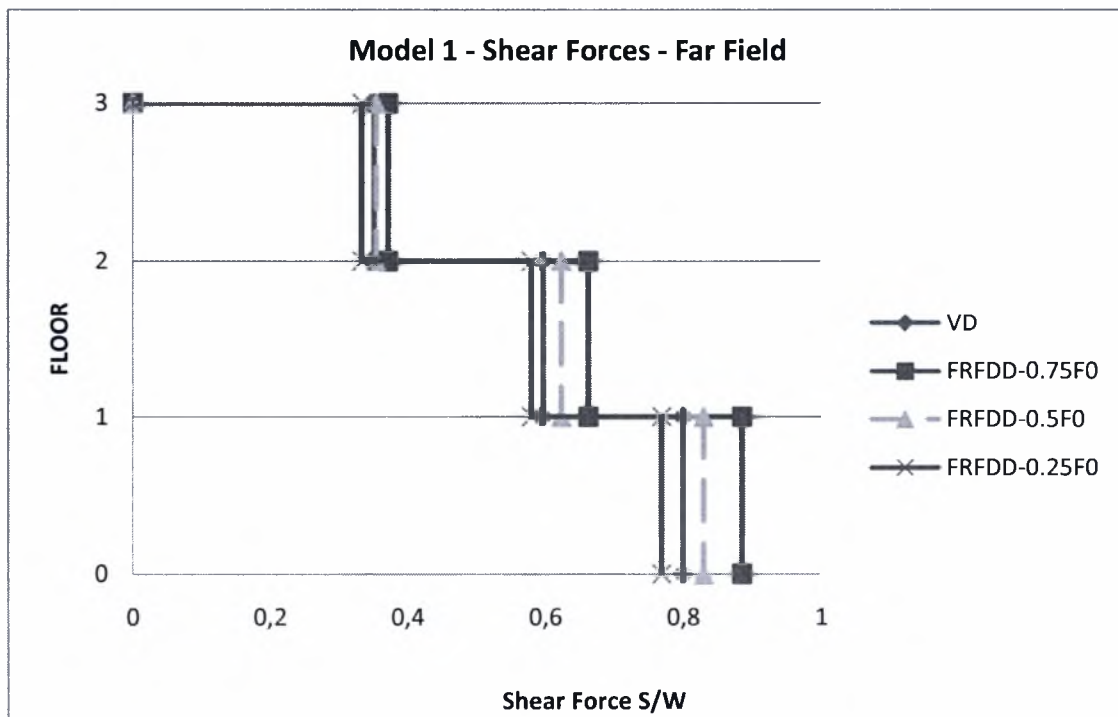
Figure 6-4 Shear Forces of Model 2 for Far Field motions

40

Results of model 1 for near fault motions.
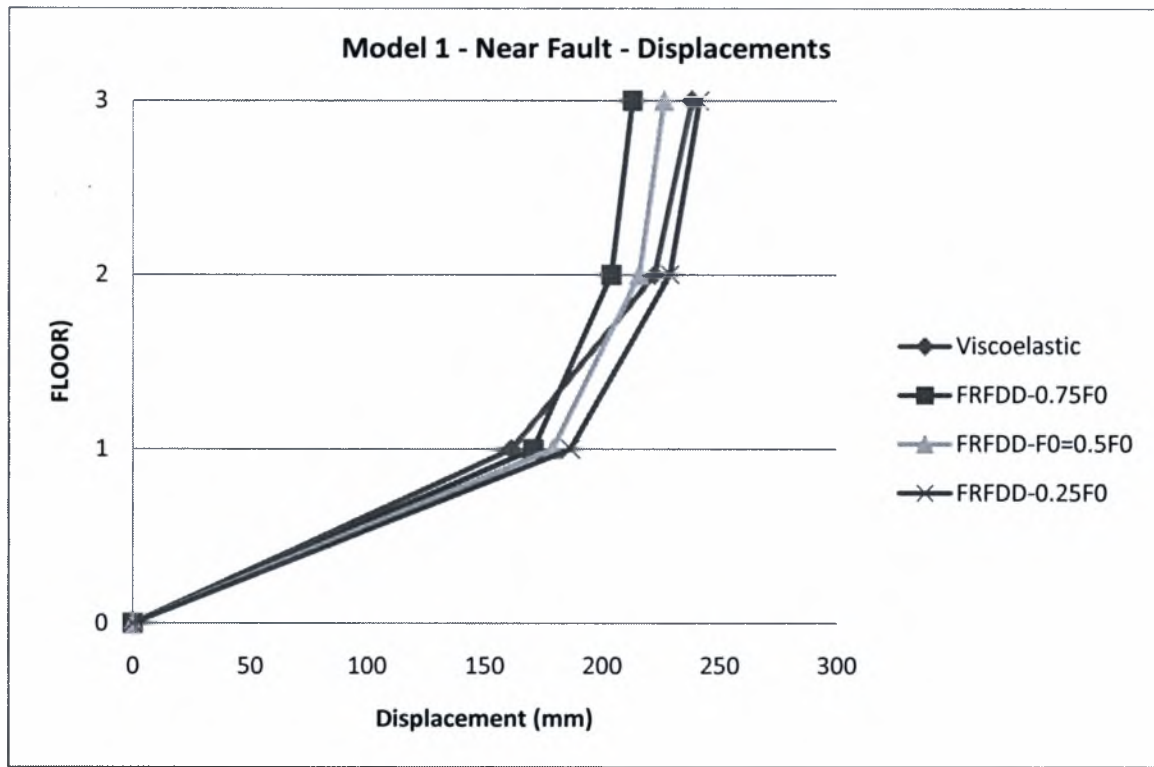
Figure 6-5 Displacements of Model 1 for Near Fault motions.
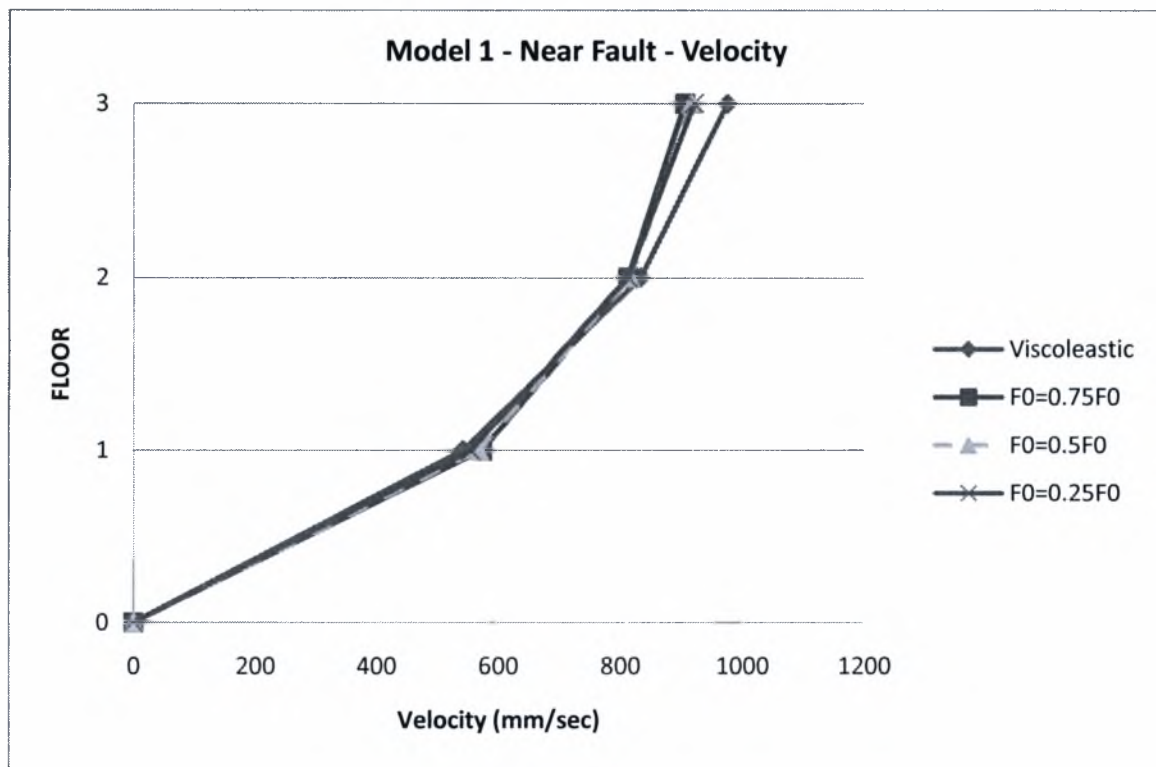
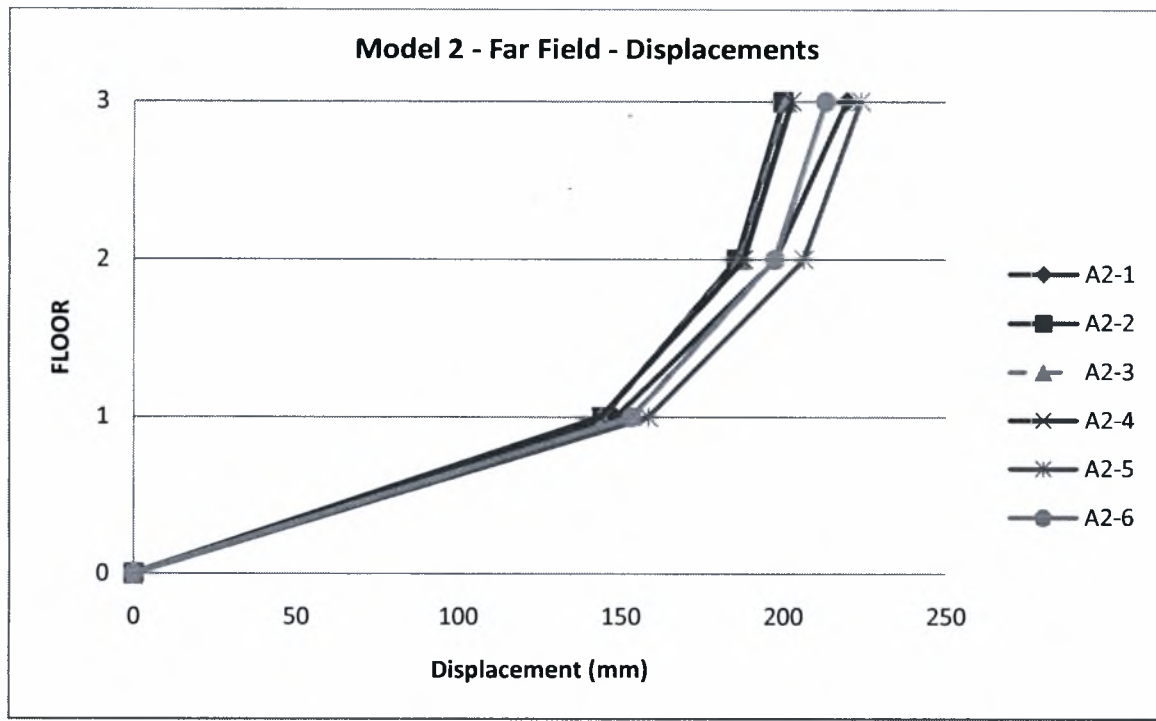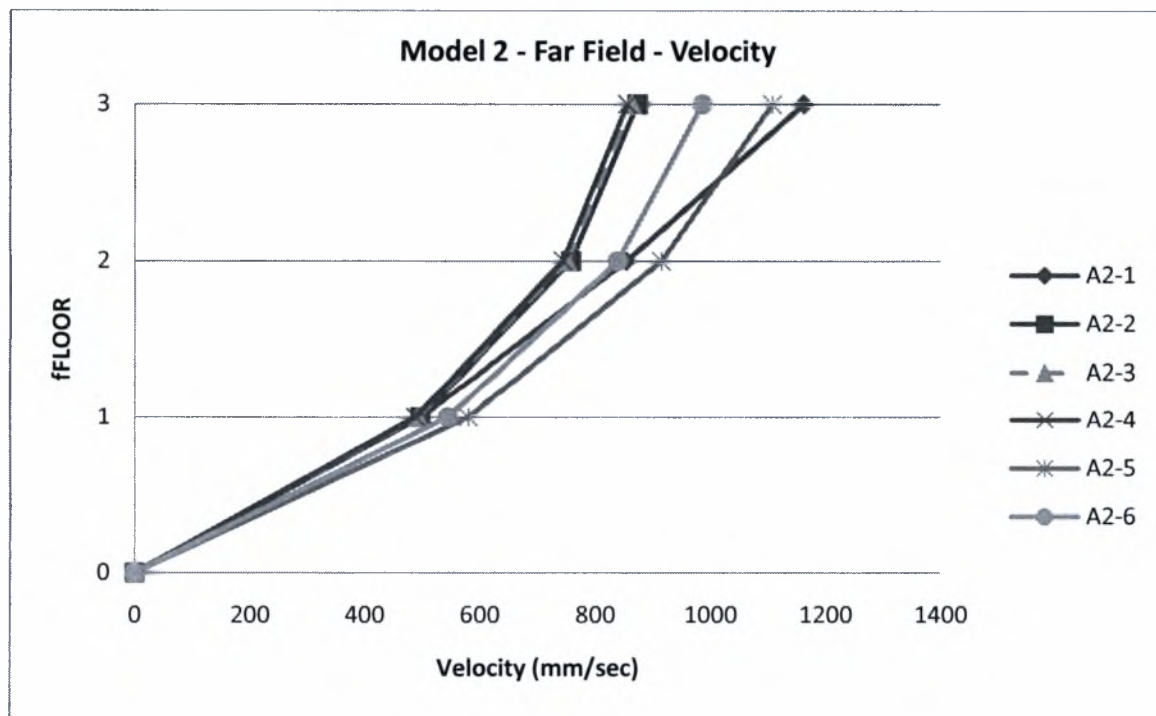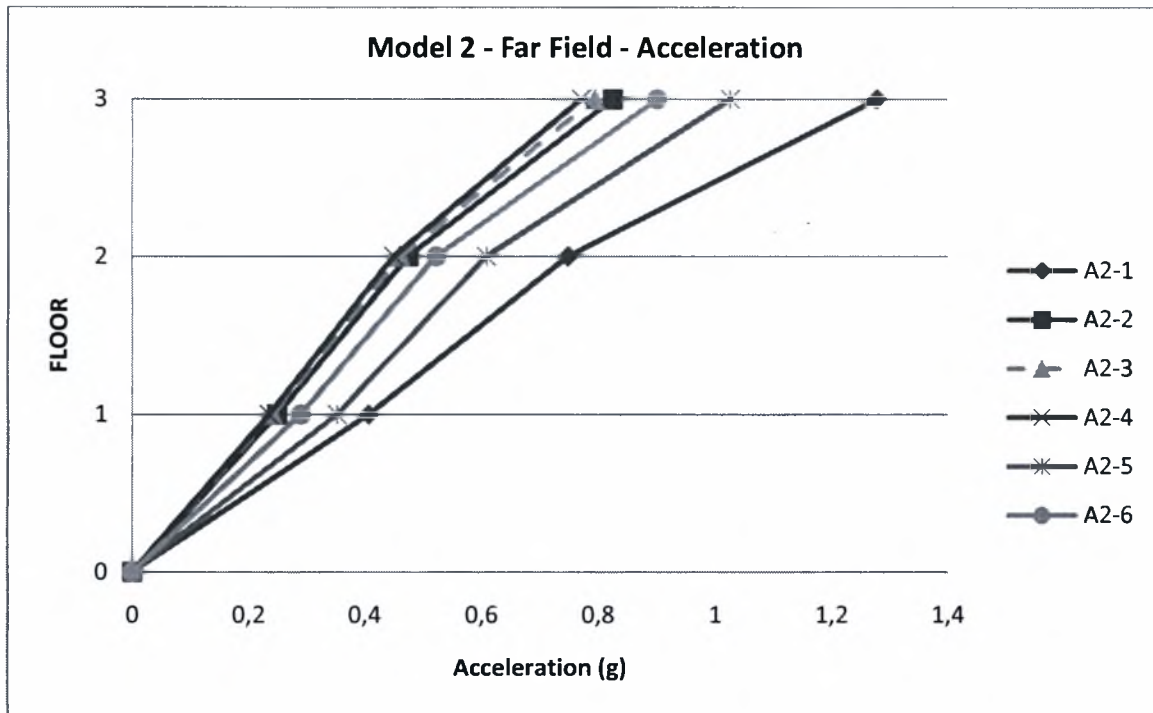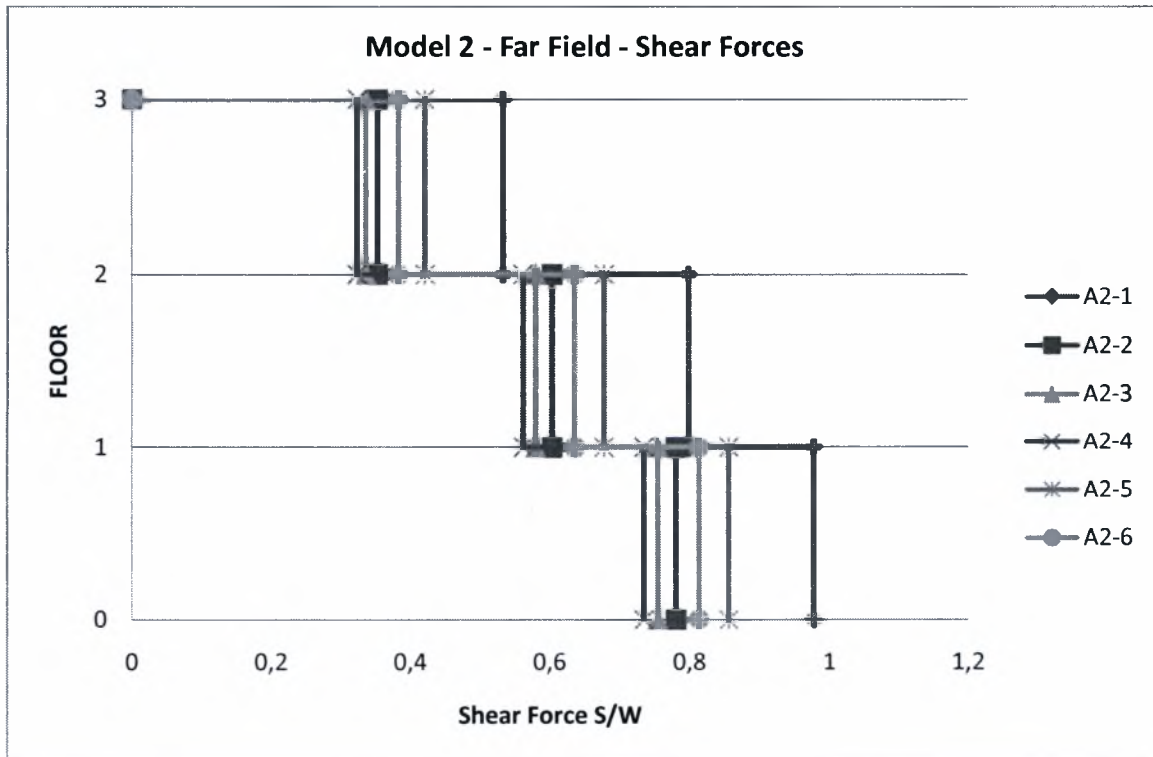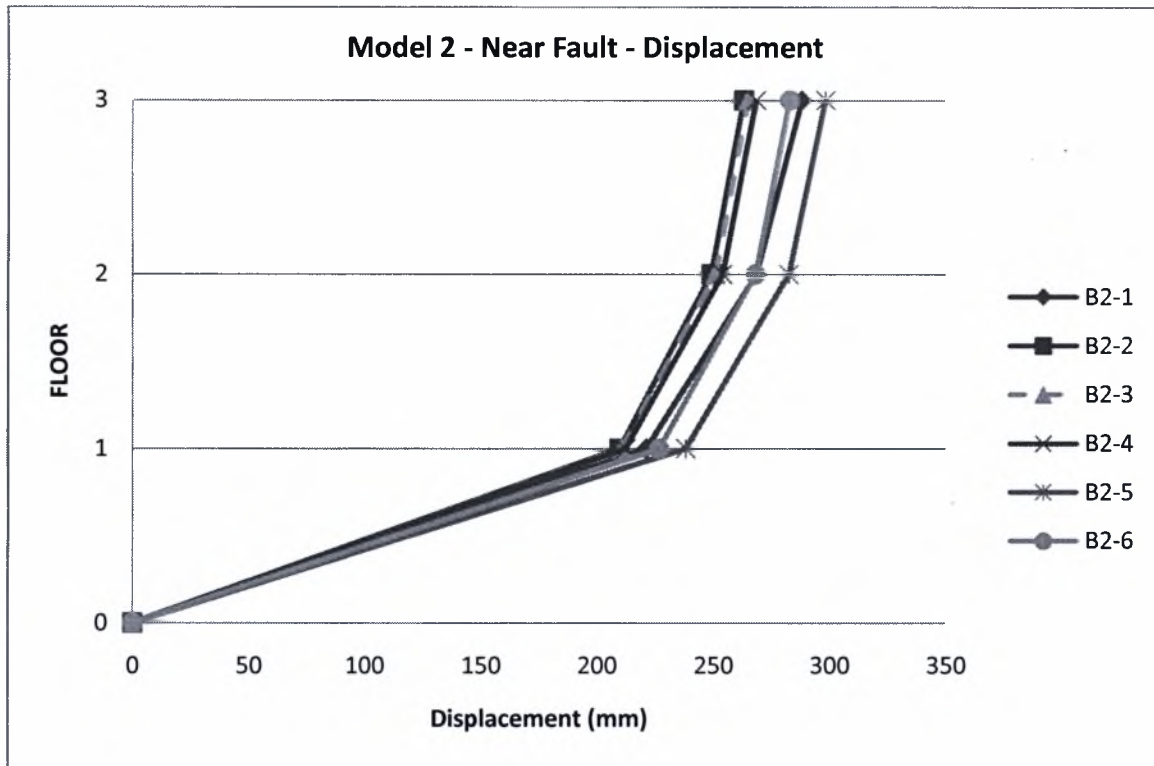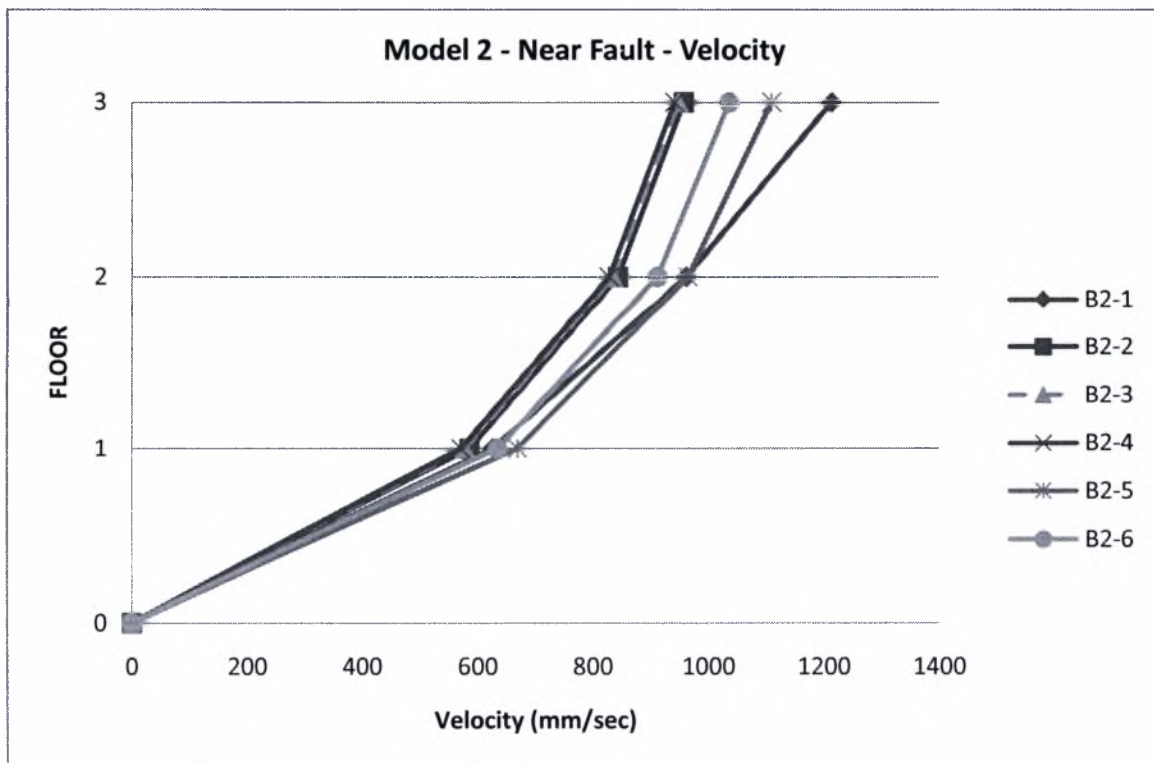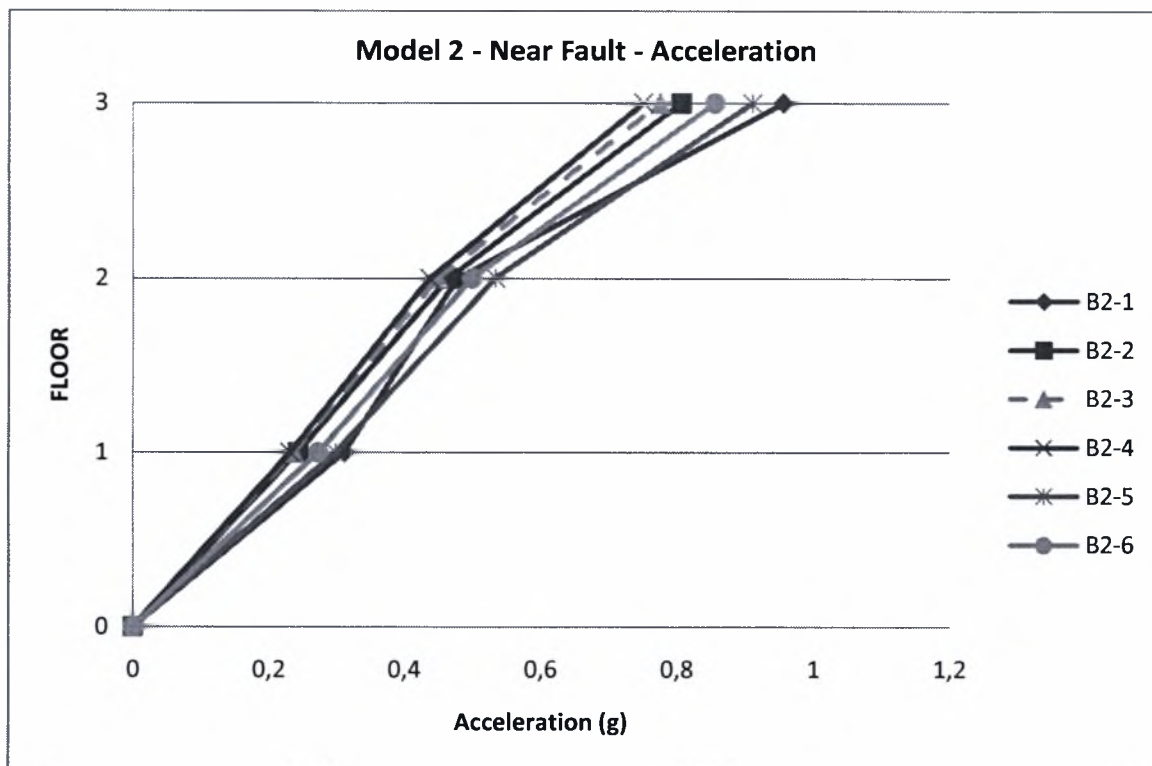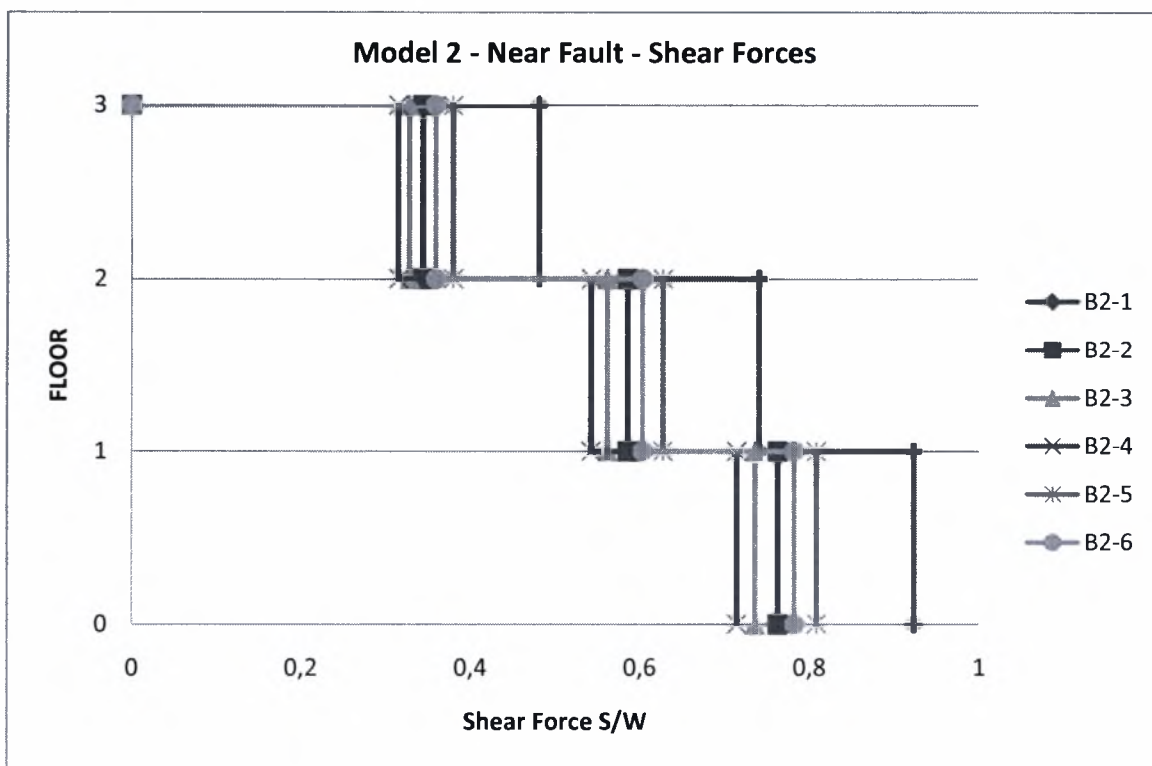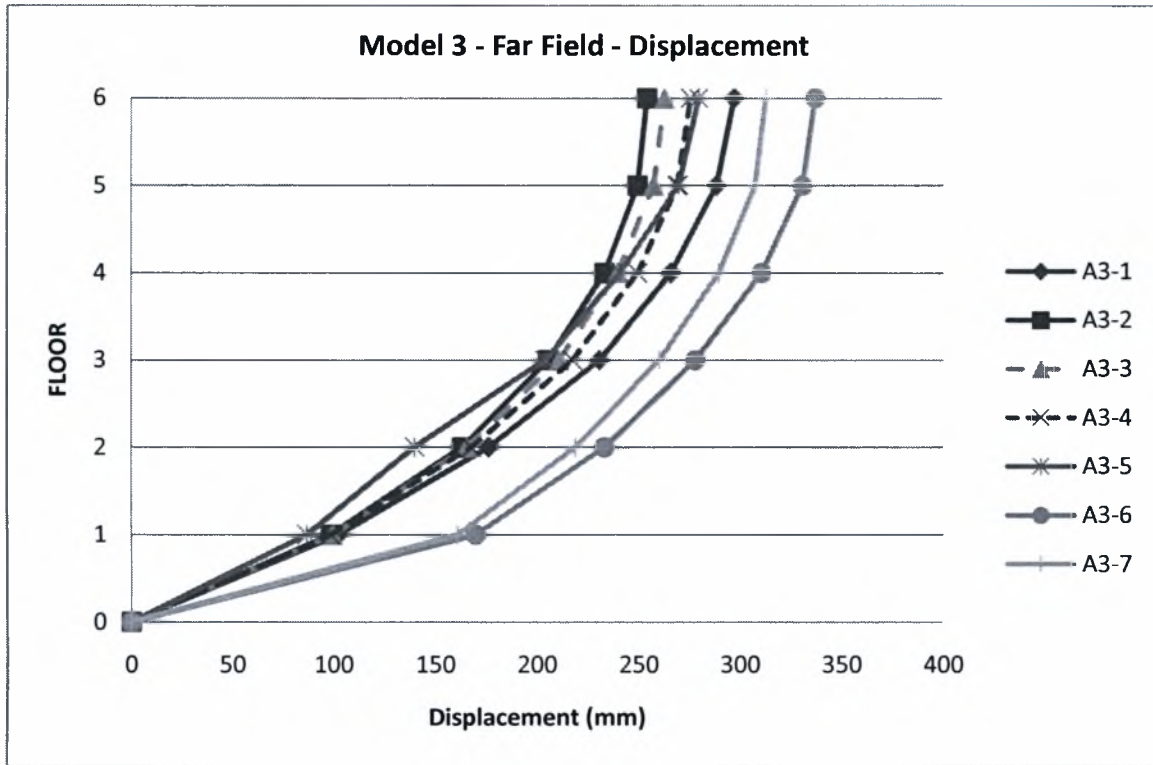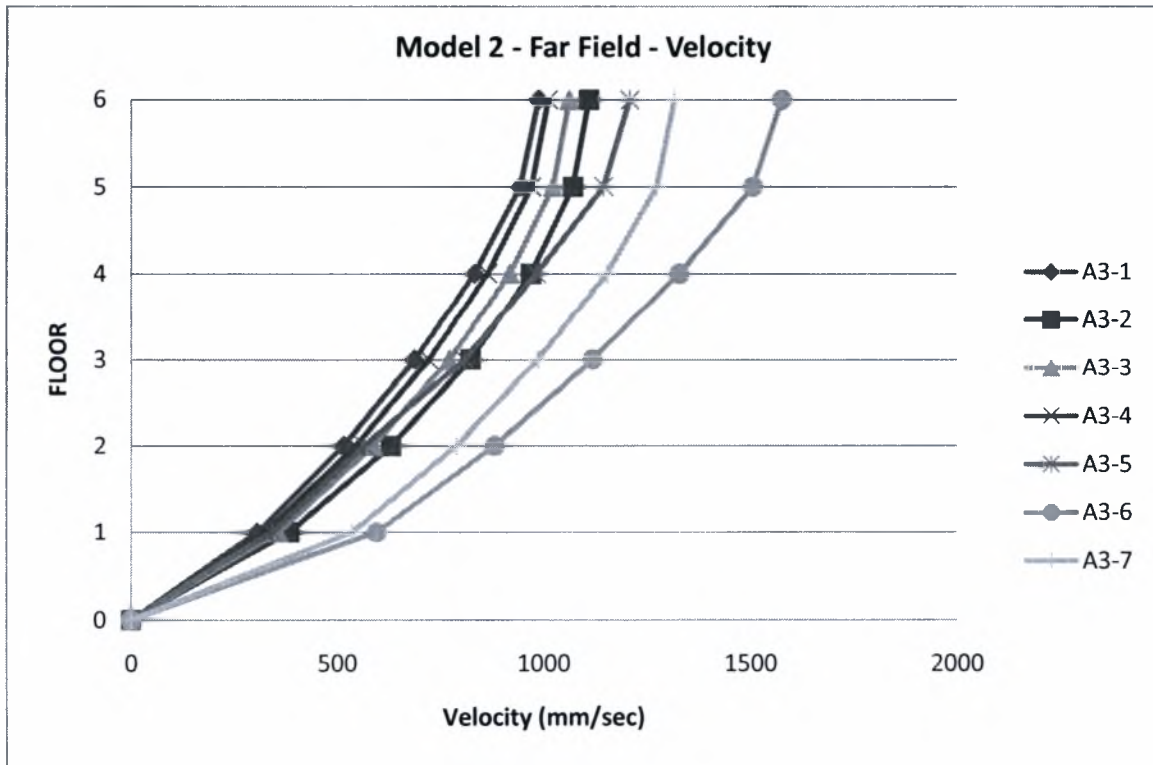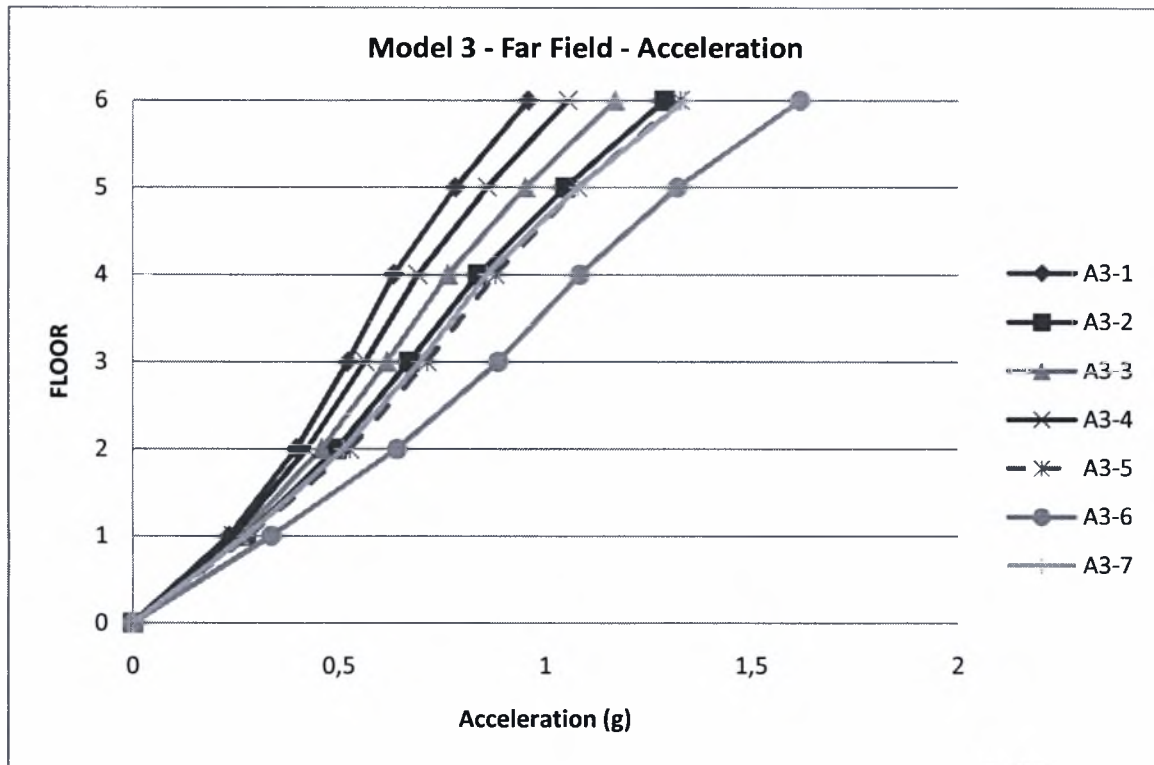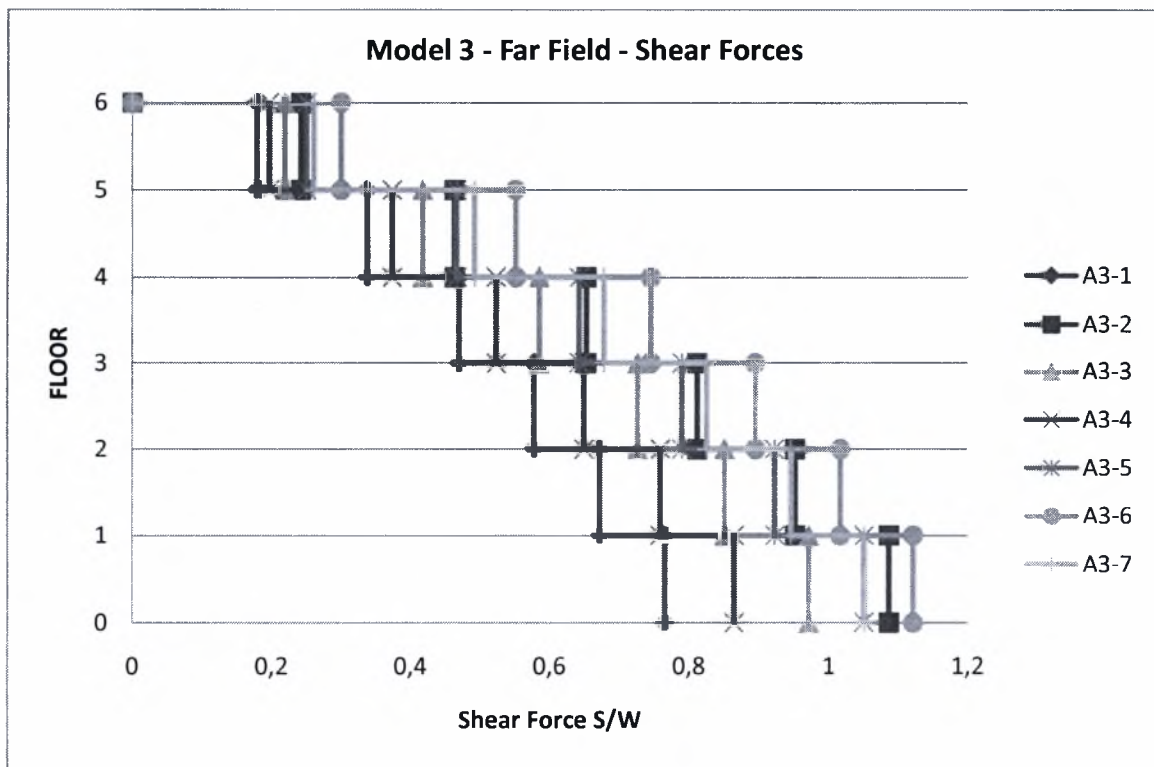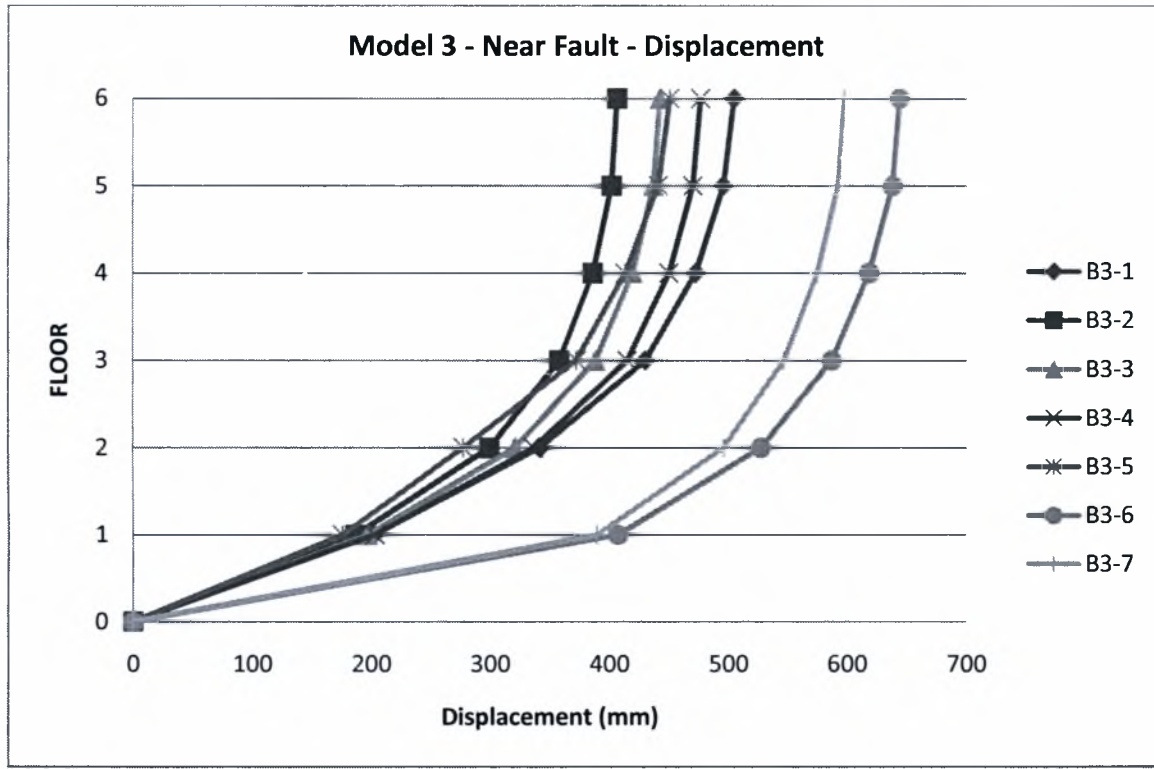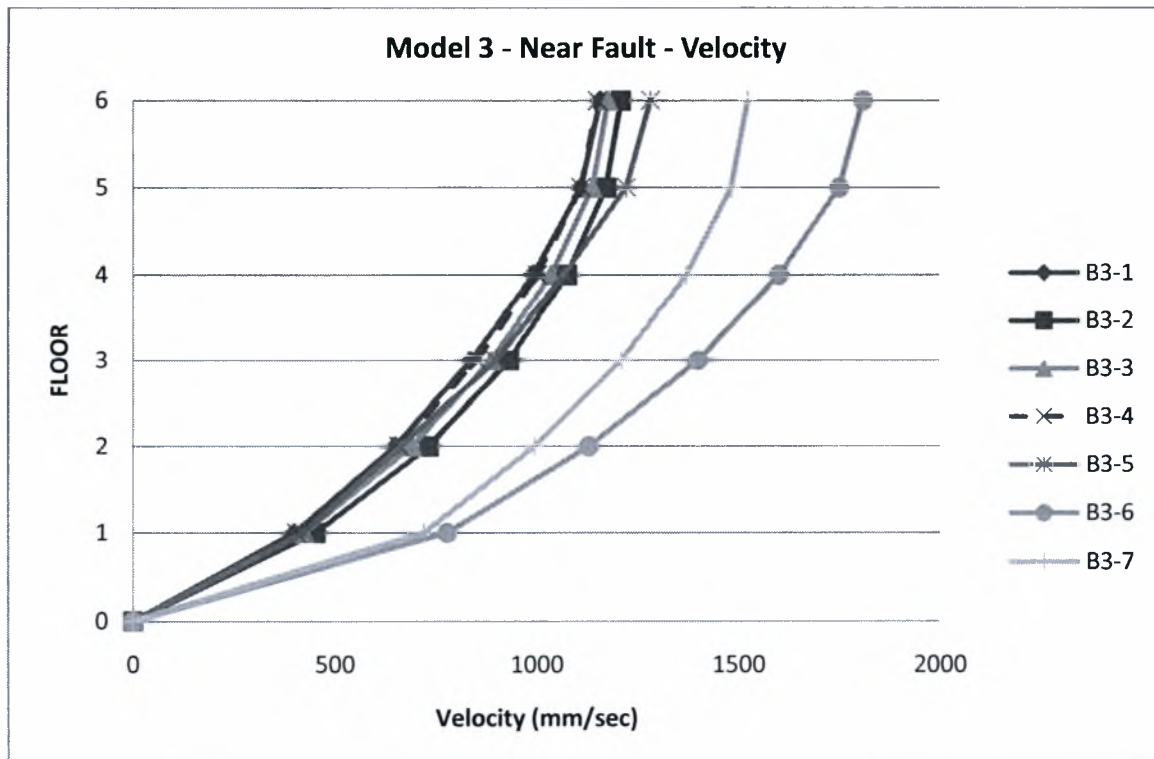**Figure 6-6 Velocities of Model 1 for Near Fault motions.**

41
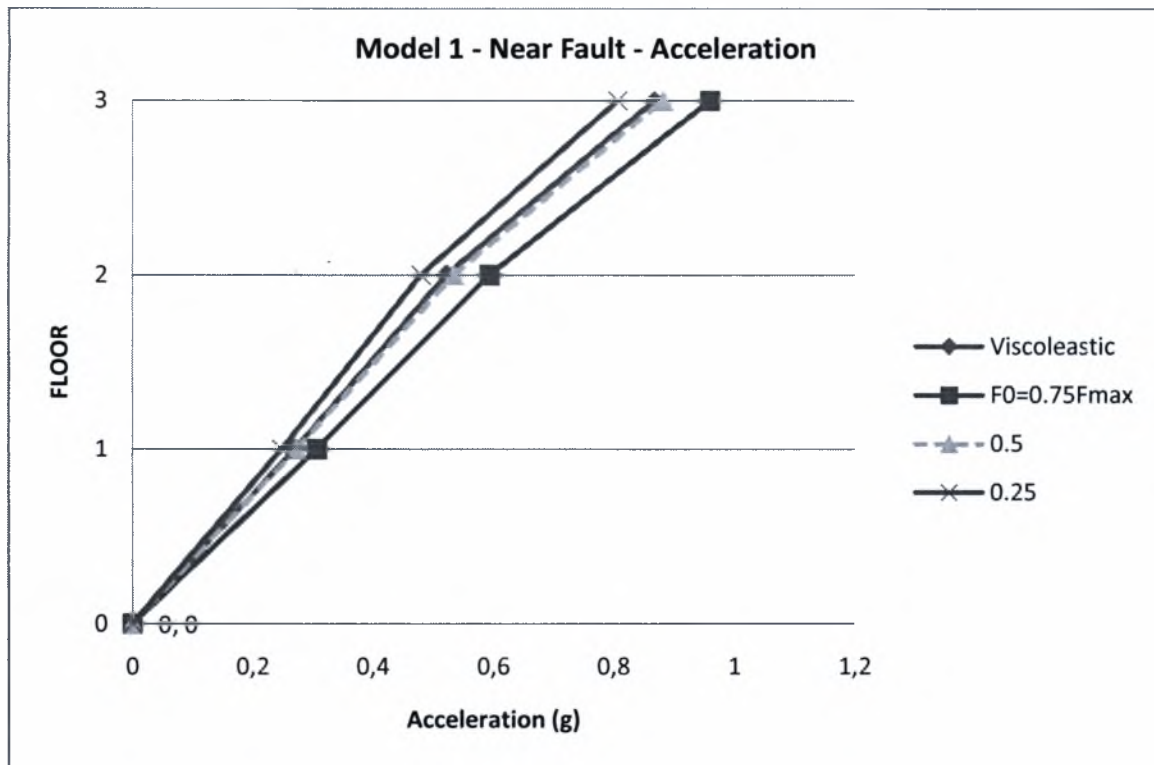
Figure 6-7 Accelerations of Model 1 for Near Fault motions.
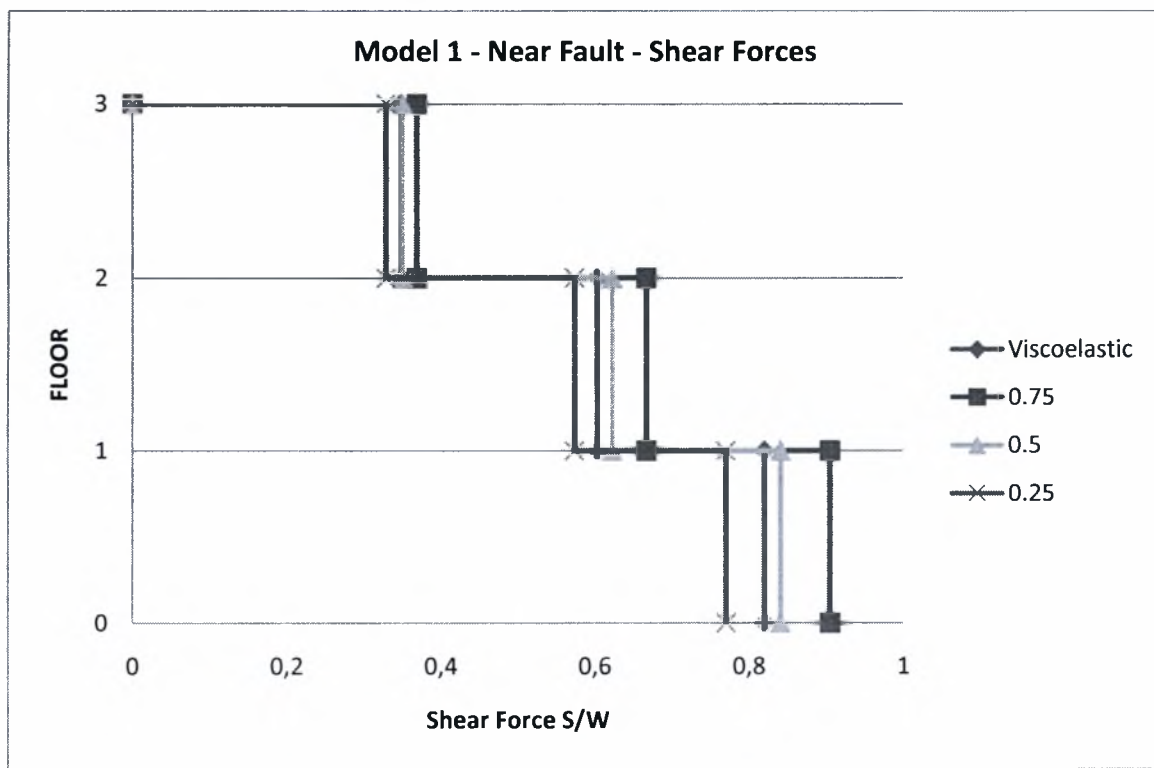
Figure 6-8 Velocities of Model 1 for Near Fault motions.

42

Results of model 2 for far field motions.

Figure 6-9 Displacements of Model 2 for Far-Field motions.

Figure 6-10 Velocities of Model 2 for Far-Field motions.

43

Figure 6-11 Accelerations of Model 2 for Far-Field motions.

Figure 6-12 Shear Forces of Model 2 for Far-Field motions.

44

Results of model 2 for near fault motions.

Figure 6-13 Displacements of Model 2 for Near Fault motions.

Model 2 - Near Fault - Acceleration

Figure 6-15 Accelerations of Model 2 for Near Fault motions.

Model 2 - Near Fault - Shear Forces

Figure 6-16 Shear Forces of Model 2 for Near Fault motions.

46

Figure 6-17 Displacements of Model 3 for Far-Field motions.

Figure 18 Velocities- of Model 3 for Far-Field motions.

Figure 19 Accelerations of Model 3 for Far-Field motions.

Figure 20 Shear Forces of Model 3 for Far-Field motions.

48

Results of model 3 for near fault motions.

Figure 6-21 Displacements of Model 3 for Near Fault motions.

Figure 6-22 Velocities of Model 3 for Near Fault motions
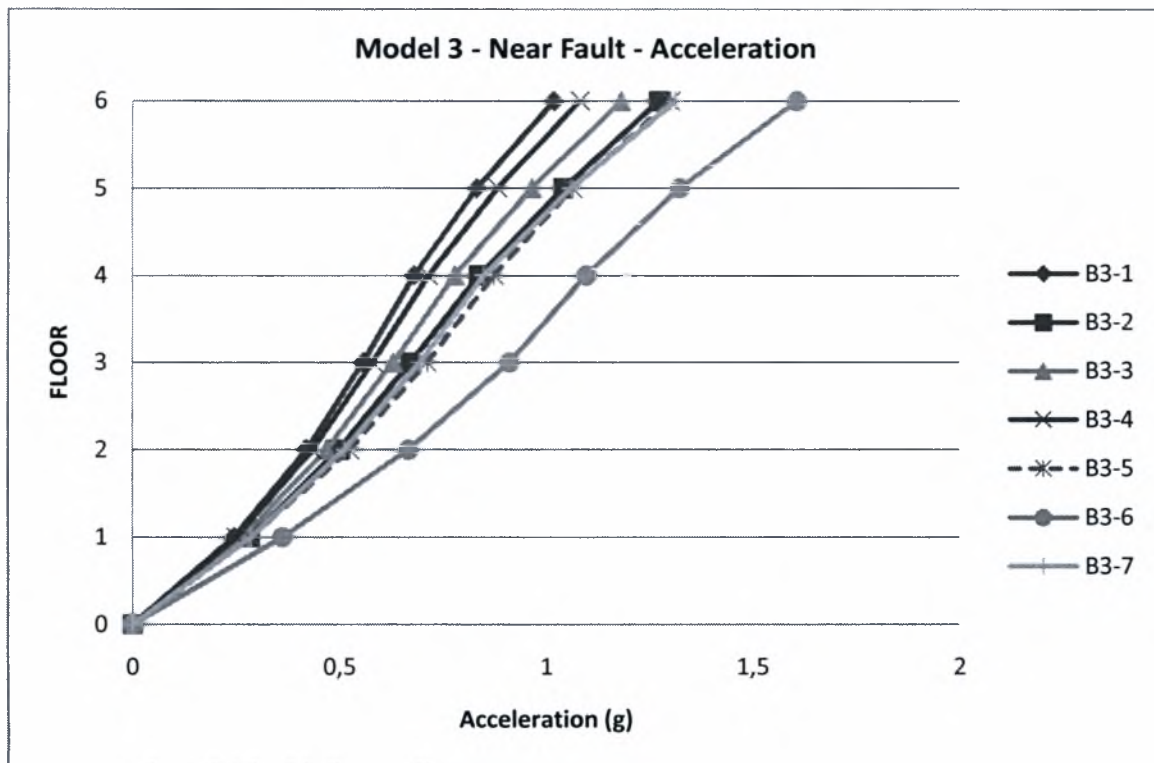
. Figure 6-23 Accelerations of Model 3 for Near Fault motions
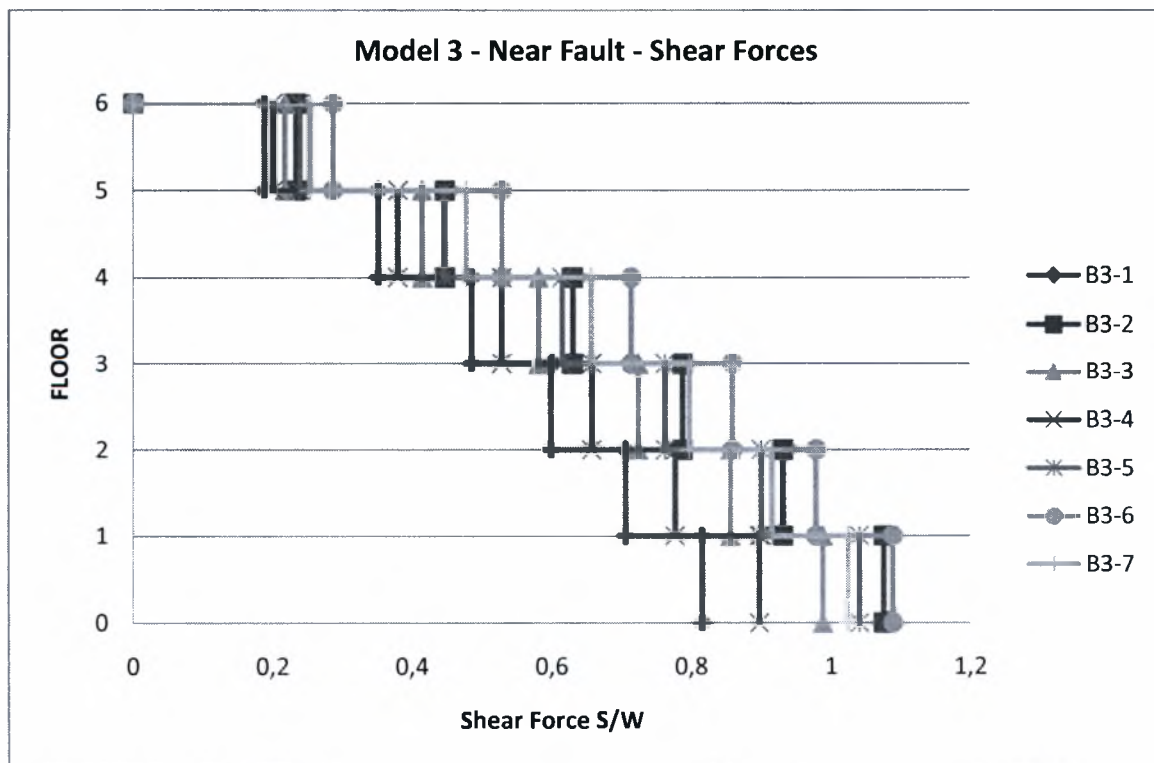
. Figure 6-24 Shear Forces of Model 3 for Near Fault motion

50

6 REFERENCES

Priestley, M. J. N., and MacRae, G. A. (1996). "Seismic testing of precast beam-to-column joint assemblage with unbonded tendons." PCI J.,Precast/Prestressed Concrete Institute, 41(1), 64–80.

Priestley, M. J. N., and Tao, J. (1993). "Seismic response of precast prestressed concrete frames with partially debonded tendons." PCI J.,Precast/Prestressed Concrete Institute, 38(1), 58–69.

Mander, J. B., Contreras R., and Garcia, R. (1998). "Rocking columns: An effective means of seismically isolating a bridge." Tech. Rep. MCEER-98-0001, Proc., U.S.–Italy Workshop on Seismic Protective Systems for Bridges, Colombia Univ. New York, 335–348.

Pekcan, G., Mander, J. B., and Chen, S. S. (1995). "The seismic response of a 1:3 scale R.C. structure with elastomeric spring dampers." Earthquake Spectra, Earthquake Engineering Research Institute, 11(2), 249–267.

Pekcan, G., Mander, J. B., and Chen, S. S. (2000b). "Balancing lateral loads using tendon-based supplemental damping system." J. Struct. Eng., 126(8), 896–905

Cheok, G. S., and Stone, W. C. (1994). "Performance of 1/3 scale model precast concrete beam-column connections subjected to cyclic inelastic loads—Report No. 4." Rep. No. NISTIR 5436, National Institute of Standards and Technology _NIST_, Gaithersburg, Md.

Mander, J. B., and Cheng, C. T. _(1997). "Seismic resistance of bridge piers based on damage avoidance design." Technical Rep. No., NCEER-97-0014, State Univ. of New York, Buffalo, N.Y.

Kwan, W.-P., and Billington, S. L. _(2003). "Unbonded posttensioned concrete bridge iers. II: Seismic analyses." J. Bridge Eng., 8_2_, 102–111.

Kurama, Y., Sause, R., Pessiki, S., and Lu, L.-W. (1999). "Lateral load behaviour and seismic design of unbonded post-tensioned precast concrete walls." ACI Struct. J., 96_4_, 622–632.

Pampanin, S. (2005). "Emerging solutions for high seismic performance of precast/prestressed concrete buildings." J. Adv. Concr. Technol., 3_2_, 202–223.

Christopoulos, C., Filiatrault, A., Uang, C. M., and Folz, B. (2002). "Posttensioned energy dissipating connections for moment-resisting steel frames." J. Struct. Eng., 128(9), 1111–1120.

Christopoulos, C., Tremblay, R., Kim, H.-J., and Lacerte, M. (2008). "Self-centering energy dissipative (SCED) bracing system for the seismic resistance of structures: Development and validation." J. Struct. Eng., 134(1), 96–107.

Tremblay, R., Lacerte, M., and Christopoulos, C. (2008) "Seismic Response of Multistory Buildings with Self-Centering Energy Dissipative Steel Braces." J. Struct. Engrg. 134, (1), 108-120

Tsopelas, P., Constantinou, M.C. "NCEER-TAISEI Corporation Research Program on Sliding Seismic Isolation Systems for Bridges-Experimental and Analytical Study of Systems Consisting of Sliding Bearings and Fluid Restoring Force/Damping Devices." Report No. NCEER 94-0014. Nat. Ctr. for Earthquake Engrg. Res., State Univ. of New York, Buffalo, NY., (1994)

Tsopelas, P., Constantinou, M. C., Kircher, C. A. and Whittaker, A. S. "Evaluation of a Simplified Methods of Analysis for Yielding Structures with Energy Dissipation Systems." Report No. NCEER 97-0012. Nat. Ctr. for Earthquake Engrg. Res., State Univ. of New York, Buffalo, NY., (1997)
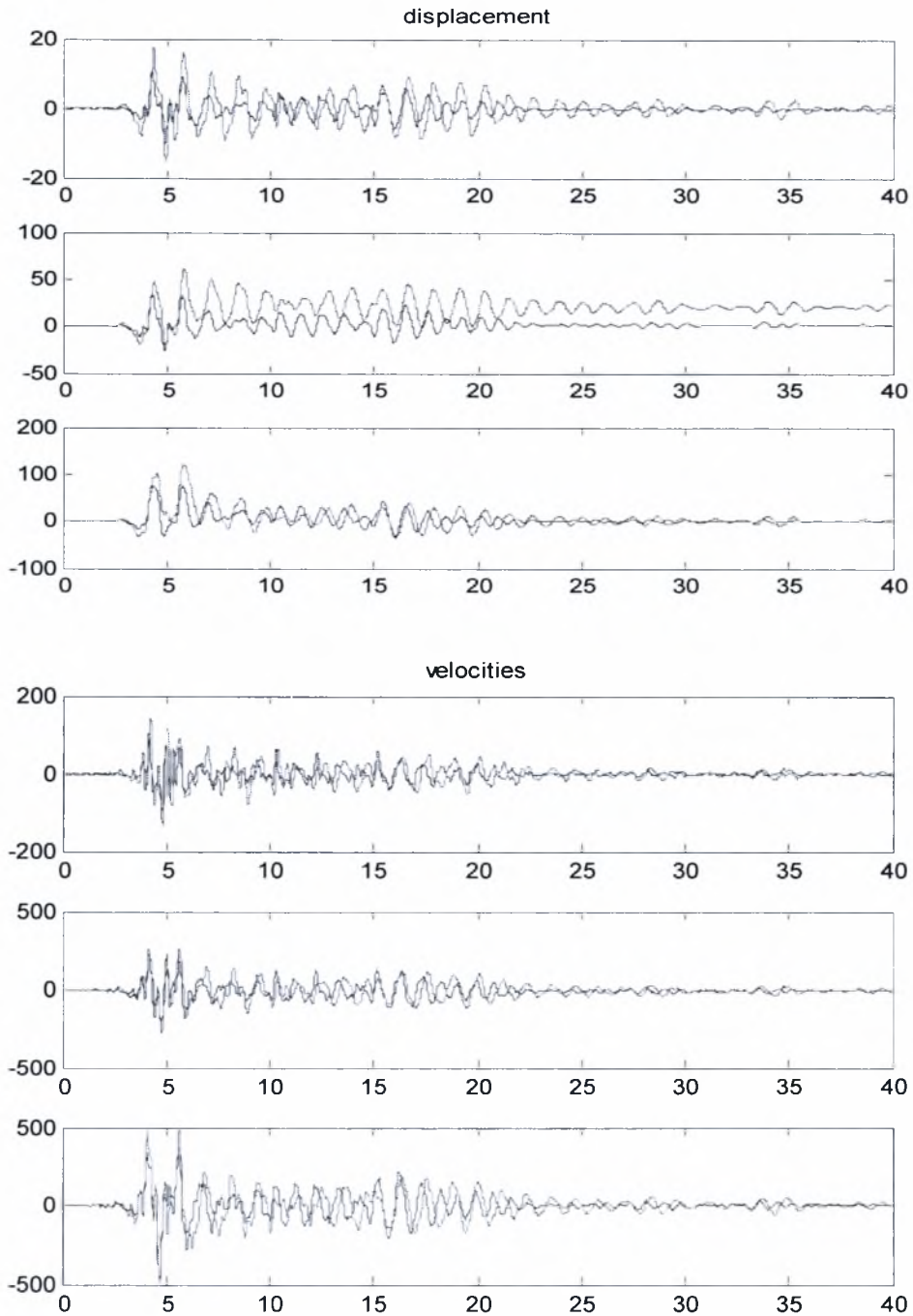
Constantinou et al. (1998)
Soong and Dargush (1997)
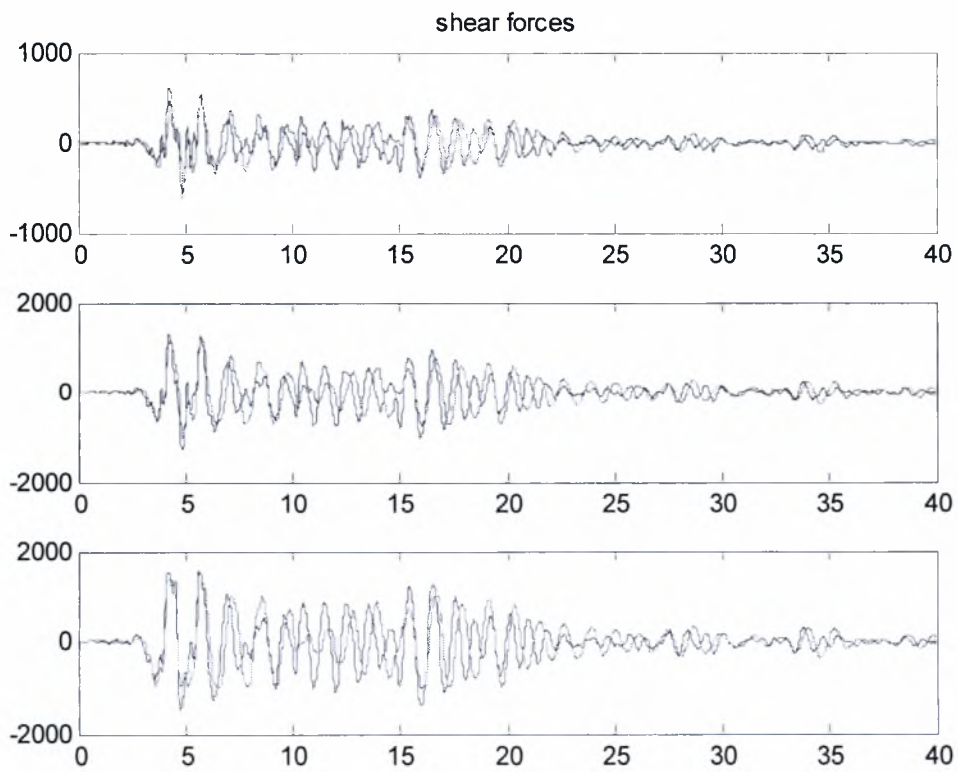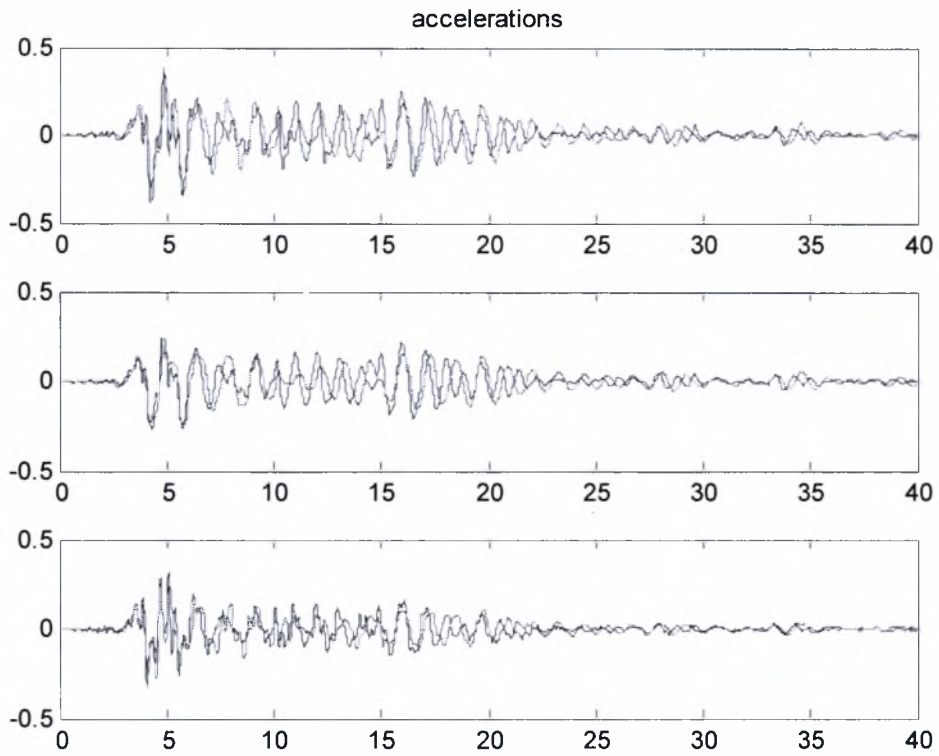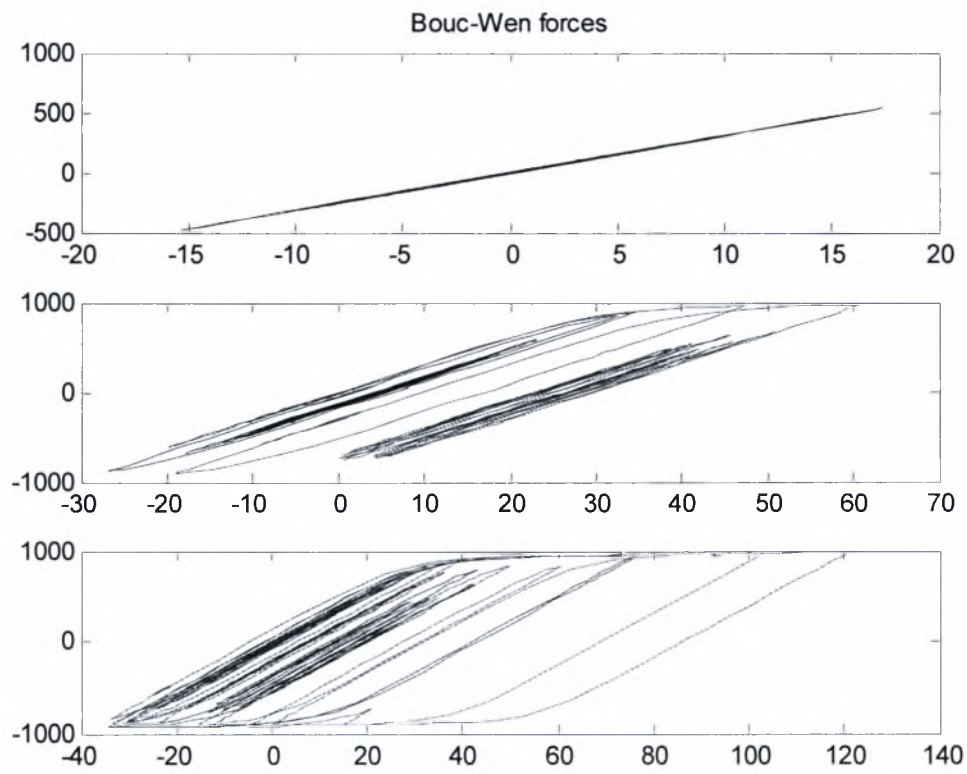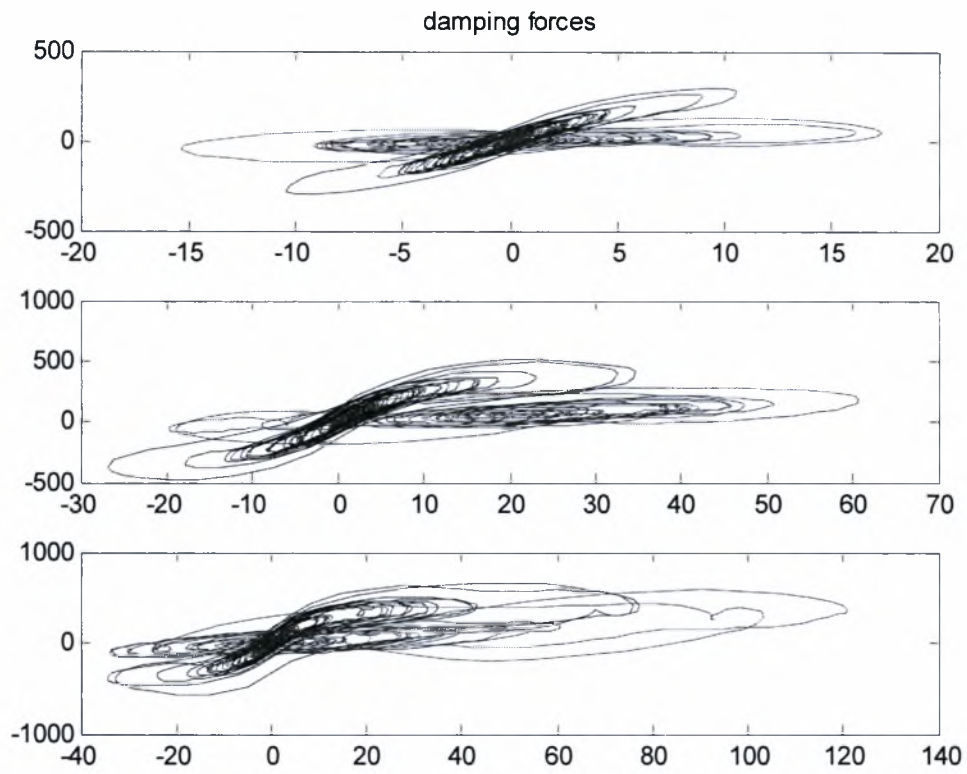Ramirez et al. (2002)

7 APPENDIX A

Herein are presented indicative the plotted time histories for the first motion for each model.

Viscoelastic – Fluid device, for F0= 0.75 Fmax.
X-axis is time (second) BLUE=Fluid device, GREEN= Viscoelastic

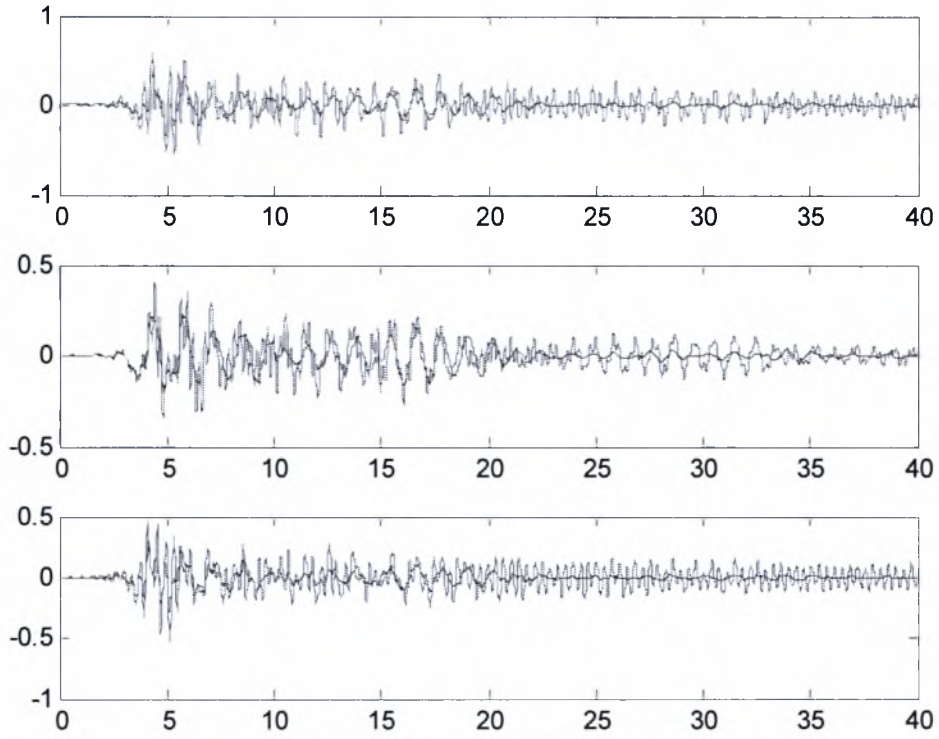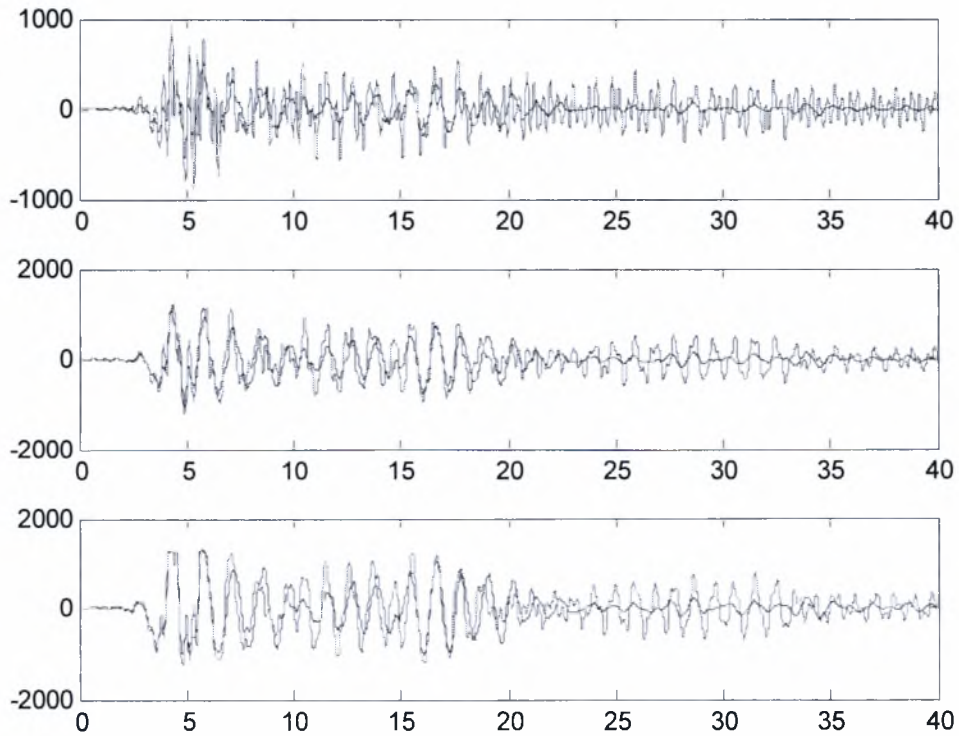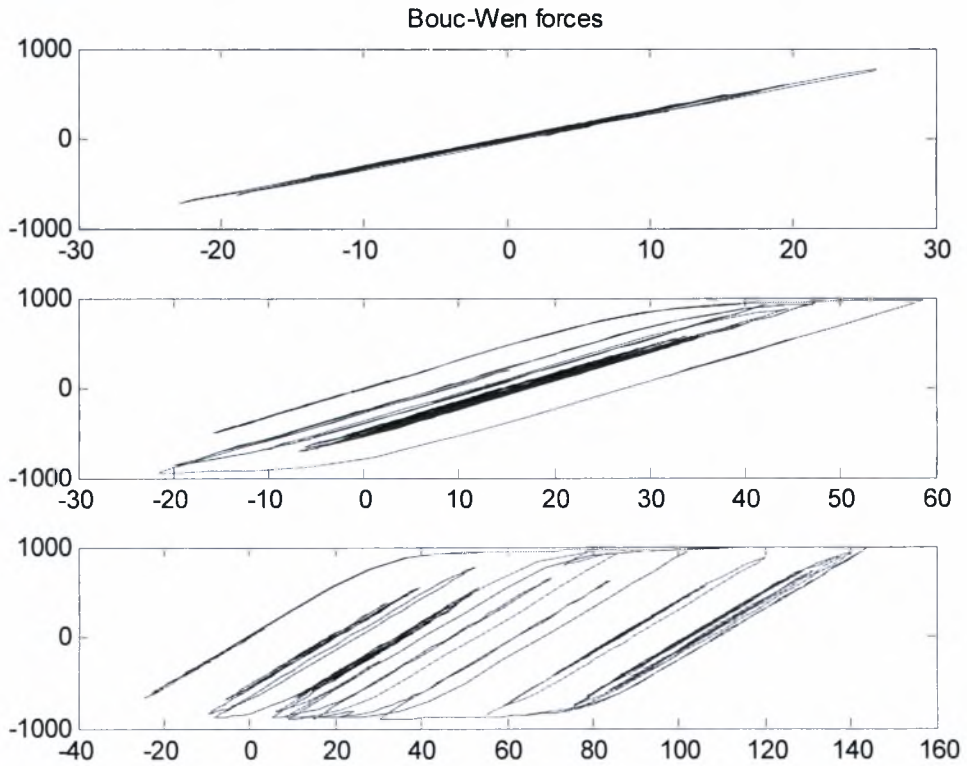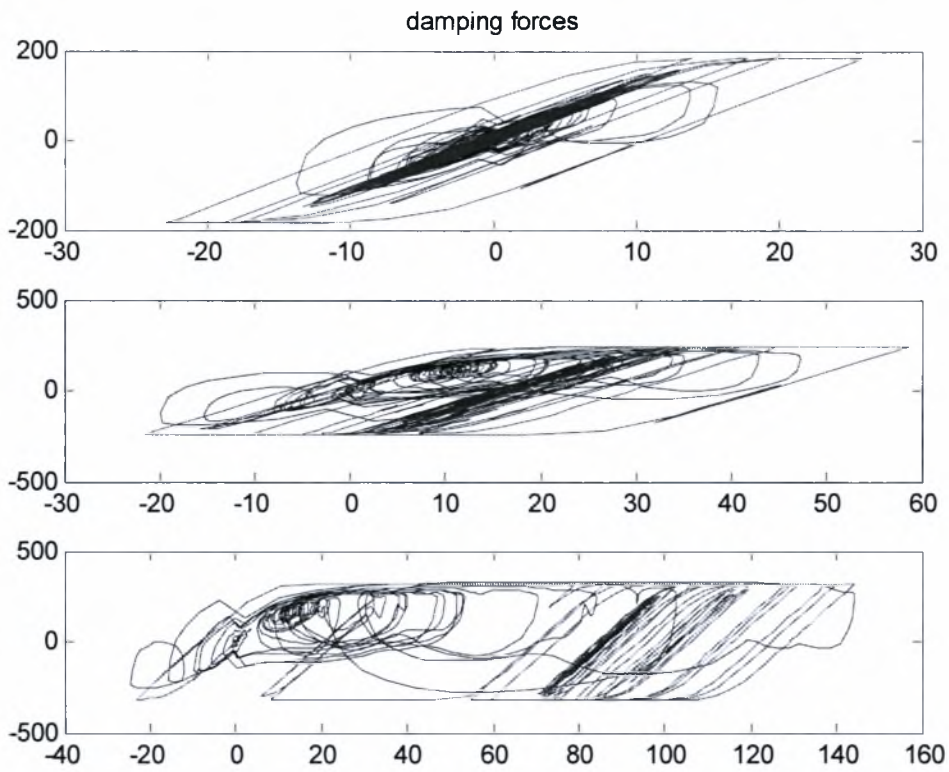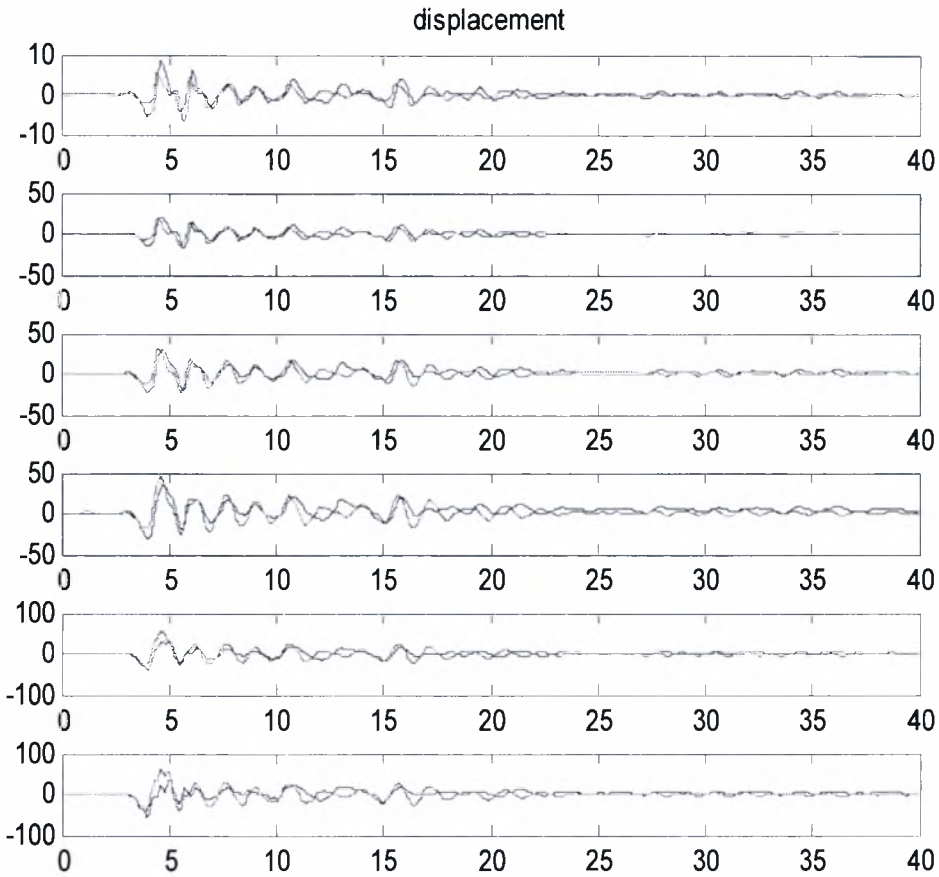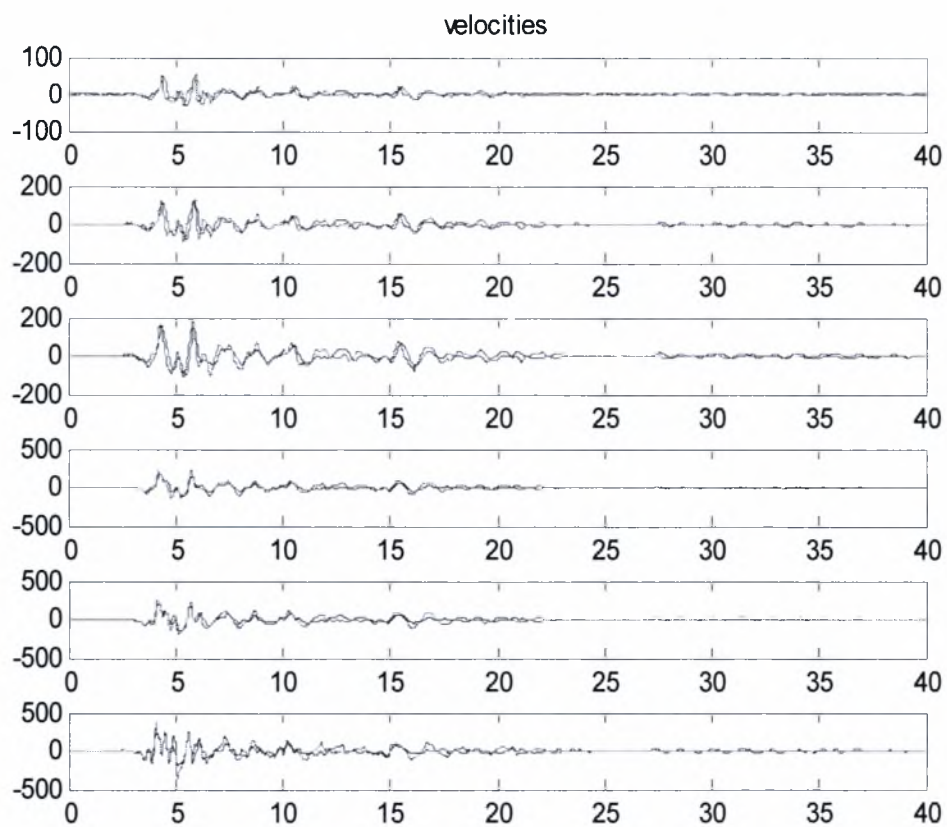accelerations

shear forces

54

damping forces

Bouc-Wen forces

55

Steel Yielding – Fluid device, for F0= 0.75 Fmax.
X-axis is time (second) BLUE=Fluid device, GREEN= Steel Yielding
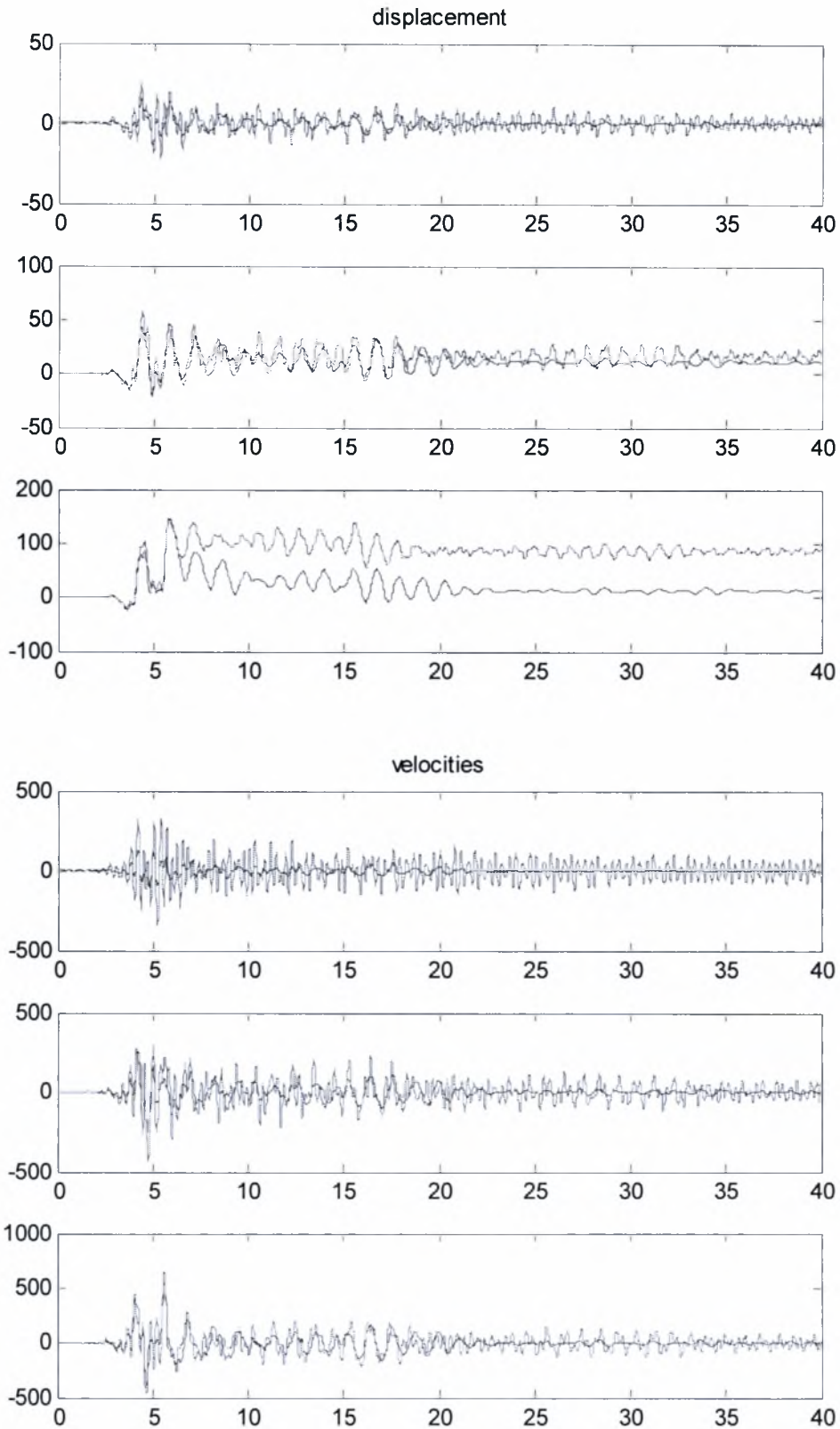
displacement
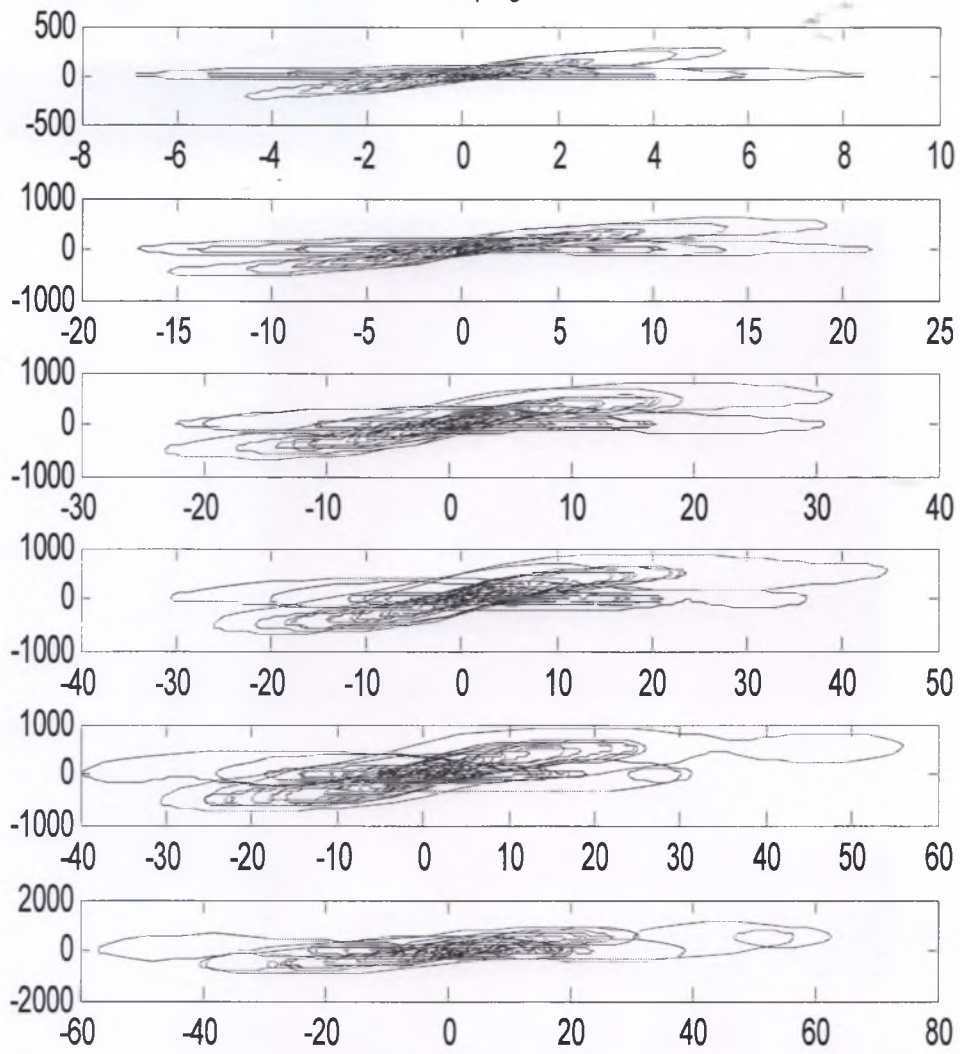

velocities

accelerations

shear forces

57

damping forces

Bouc-Wen forces

58

Steel Yielding – Fluid device, for F0= 0.75 Fmax.
X-axis is time (second) BLUE=Linear Viscous, GREEN= Fluid device

displacement

velocities

accelerations

60

shear forces

Bouc-Wen forces

61

Damping forces